Calendar-dated glacier variations in the Western European Alps during the Neoglacial: the Mer de Glace record, Mont Blanc massif

Melaine Le Roy, Kurt Nicolussi, Philip Deline, Laurent Astrade, Jean-Louis Édouard, Cécile Miramont, Fabien Arnaud

https://doi.org/10.1016/j.quascirev.2014.10.033

Calendar-dated glacier variations in the Western European Alps during the Neoglacial: the Mer de Glace record, Mont Blanc massif

Melaine Le Roy [a], Kurt Nicolussi [b], Philip Deline [a], Laurent Astrade [a], Jean-Louis Edouard [c], Cécile Miramont [d], Fabien Arnaud [a]

[a] EDYTEM, Université de Savoie, CNRS, 73376 Le Bourget du Lac, France
[b] Institute of Geography, University of Innsbruck, 6020 Innsbruck, Austria
[c] Centre Camille Julian, Aix-Marseille Université, CNRS, 13094 Aix-en-Provence, France
[d] IMBE, Aix-Marseille Université, CNRS, 13545 Aix-en-Provence, France.

Highlights

- We present a new dendro-based Neoglacial glacier record for the European Alps
- Ten glacier advances were calendar-dated during the last 4000 years
- Timing of Neoglacial advances proposed here broadly agrees with previous works
- Minor differences between glacier records could arise from glacier response time

Abstract

Holocene glacier records from the Western European Alps are still extremely sparse despite existence of some well-suited sites to use dendrochronology to constrain pre-Little Ice Age (LIA) glacier advances. Based on the analysis of more than 190 glacially buried *Pinus cembra* subfossil logs and wood remains from the Mer de Glace lateral moraine in the Mont Blanc massif, we present the first dendro-based and calendarically dated Neoglacial glacier chronology for this area. Main burial events, interpreted as glacier advances, are recorded between 1610 and 1544+ BC, between 1230+ and 1105+ BC, after 962+/937+ BC, around 802 to 777 BC, after 608+ BC, between 312 and 337 AD, after 606+ AD, between 1120 and 1178 AD, around 1296 AD, and after 1352+ AD – predating historically-known late LIA maxima. Magnitude of the advances shows increasing trend, culminating with near-Neoglacial maxima during the 7th and 12th-13th century AD glacier advances, and a first LIA/ Neoglacial maximum reached in the second half of the 14th century AD. Due to uncertainties about original growth location of some trees, these dates are mostly considered as maximum-

limiting ages for glacier advances. The pattern of Neoglacial events described here is coherent with Central and Eastern Alps glacier chronologies indicating marked synchronicity of late Holocene glacier variability and forcing at a regional scale. The Mer de Glace record also confirms the link between the timing of sediment erosion in a high-elevated glaciated alpine catchment and subsequent deposition in the pre-alpine lake Le Bourget. These results highlight the great potential of dendrochronology to establish high-resolution glacier fluctuation records even in the French Alps.

Keywords: glacier chronology, Neoglacial, Holocene, dendrochronology, subfossil wood, Mer de Glace, Mont Blanc, Western Alps

1. Introduction

Holocene climate variability has been subject to increasing attention for about two decades (Mayewski et al., 2004; Wanner et al., 2008), especially as evidences emerged of a late 20th/early 21st century warming of unprecedented nature on the last millennium timescale – at least as regards the European Alps (*e.g.* Büntgen and Tegel, 2011; Trachsel et al., 2012). Accurate knowledge of both amplitude and timing of Holocene climate change is thus necessary to assess the natural variability range, to identify the main forcings and to model the future climate (Jansen et al., 2007; Humlum et al., 2011; Wanner et al., 2011).

High-altitude environments are sensitive to slight change in forcing and a variety of proxies have been investigated to reconstruct Holocene climate variability in the European Alps: paleoecological indicators of the treeline ecotone altitudinal variation and composition (Haas et al., 1998; Tinner and Theurillat, 2003; Nicolussi et al., 2005; Blarquez et al., 2010; Berthel et al., 2012), lithological and geochemical lake-sediment properties (Schmidt et al., 2008; Giguet-Covex et al., 2012), pollen and chironomid assemblages (David, 1997, 2010; Heiri et al., 2003; Ilyashuk et al., 2011), and stable isotopes measured in speleothems (Vollweiler et al., 2006; Boch and Spötl, 2011). Limitations of such studies could be either: (i) their relatively weak chronological constraints, (ii) reconstruction uncertainties resulting from *proxy* calibration, and (iii) potentially marked anthropogenic impact, hindering identification of climate signal – especially during the second part of the Holocene.

Alpine glaciers are widely recognized as reliable indicators of climate variations on inter-annual to multi-millennial timescales (Denton and Karlen, 1973; Hoelzle et al., 2003; Vincent

et al., 2004; Beedle et al., 2009). Glacier length changes represent a mixed signal of the variations in summer temperature and winter accumulation (mass-balance forcings) delayed by a time lag (Johannesson et al., 1989; Müller, 1988). They have been successfully used to infer equilibrium line altitude (ELA) and temperature variations (e.g. Leclerq and Oerlemans, 2012). Beyond the instrumental period, glacier variation reconstructions rely on documentary evidences for the last few centuries and on glacio-geomorphological (i.e. dating of moraine succession) or glacio-lacustrine investigations for the whole Holocene period.

To test for potential synchronicity of past climatic events through correlation – and by the way, to assess palaeo-circulations patterns – glacier chronologies have to be at high-resolution, i.e. relatively continuous with information at a decadal or sub-decadal scale (Winkler and Matthews, 2010; Kirkbride and Winkler, 2012). Beyond the last few centuries this goal can only be achieved either by dendrochronological calendar dating of glacially-sheared or buried subfossil tree remains in glacier forefields (Luckman, 1995; Nicolussi and Patzelt, 2001; Holzhauser et al., 2005; Wiles et al., 2011) or by a tight constraint on glacier-fed lake sediment deposition (Leeman and Niessen, 1994; Bakke et al., 2010). However, relatively few lacustrine settings have been analysed in the Alps, unlike other glaciated regions (e.g. Dahl et al., 2003). Terrestrial-based glacier chronologies have high climatic reconstruction potential but must be evaluated with regard to their representativeness. End-moraine ridge stratigraphy most often lacks continuity and records only a part of the effective glacier advances (Gibbons et al., 1984; Kirkbride and Brazier, 1998; Kirkbride and Winkler, 2012). This is especially true since the LIA cold period led to one of the most prominent Holocene advance in the Northern Hemisphere (Davis et al., 2009). A way to overcome this problem to some extent is to study lateral moraine stratigraphy, providing a more complete picture of successive Neoglacial advances (Röthlisberger and Schneebeli, 1979; Osborn, 1986; Holzhauser and Zumbühl, 1996; Osborn et al., 2001; 2012; 2013; Koch et al., 2007; Jackson et al., 2008; Reyes and Clague, 2004). The Neoglacial is defined here as the second part of the Holocene during which alpine glaciers experienced repeated advances of near-Holocene maxima amplitude, depending on their relative response time.

The European Alps are among the best-documented regions worldwide concerning the Holocene glacier variations at different timescales (Nicolussi and Patzelt, 2001; Holzhauser et al., 2005; Joerin et al., 2006; 2008; Nicolussi et al., 2006; Nussbaumer et al., 2007; Holzhauser, 2010; Goehring et al., 2011; 2012; Nicolussi and Schlüchter, 2012; Nussbaumer and Zümbuhl, 2012). Indeed, distribution of the dated sites is spatially heterogeneous: unlike Central and Eastern Alps where glacio-geomorphological studies have been conducted since

101 the 1960s (see Ivy-Ochs et al., 2009 for a comprehensive review), there have been so far very
102 few such studies in the French Alps despite their current glaciation (ca. 15 % of the Alpine
103 glacier area; Paul et al., 2011) and their location with respect to zonal circulation (**Fig. 1A**).
104 The present study aims to fill this gap and to propose a precise chronology of glacier
105 variations in the Mont Blanc massif (MBM) for the Neoglacial period based on dating of
106 glacially buried subfossil wood material in the moraines of Mer de Glace.
107
108 **Fig. 1**
109
110 ## 2. Study site
111
112 Mer de Glace (hereafter MdG; 45°55'N, 06°55'E) is the largest glacier in the French Alps,
113 covering 30.6 km^2 (without including former tributary Glacier de Talèfre; 2008 data: Gardent
114 et al., 2014) and flowing along 12 km between 4070 m and 1520 m a.s.l. (**Fig. 1B**). MdG
115 *sensu stricto* corresponds to the 5-km-long distal area of the glacier. Maximum tongue
116 thickness reached 420±10 m in 1961 at the Glacier du Tacul, downstream the Séracs du Géant
117 icefall (bedrock map in Lliboutry and Reynaud, 1981) and remains ca. 380 m today at this
118 location. Thickness decrease downstream to ca. 160 m today near Les Echelets and ca. 90 m
119 right from the Montenvers. Average ELA was 2880 m for five of the main north-facing MBM
120 glaciers, among which Glacier de Leschaux, over the period 1984-2010 (Rabatel et al., 2013).
121 Mean annual temperature and precipitation were 6.5°C and 1238 mm, respectively, at nearby
122 Chamonix-Le Bouchet station (1054 m a.s.l.) for the period 1961-1990 (Météo France data).
123 The MdG catchment is formed by granite of Late Hercynian age (Bussy and von Reumer,
124 1993; Leloup et al., 2005). Debris-supply to the glacier tongue mainly results from rockfalls
125 in the accumulation area (e.g. Ravanel et al., 2010) and paraglacial reworking of till material
126 from the lateral moraines. Since the end of the LIA, the debris cover onto the MdG *s.s.*
127 expanded (Deline, 2005): 51% of the glacier ablation zone was debris-covered in 2008
128 (Deline et al., 2012). Thinning of the tongue has strongly accelerated over the last two
129 decades and reached ca. 4 m a^{-1} since 2000 (Berthier et al., 2004; Berthier and Vincent, 2012).
130 This results in a 65 m lowering of the tongue right from Montenvers since the mid-1980s.
131
132 **Fig. 2**
133

The right lateral moraine (RLM) of MdG is a typical example for marginal deposits of large temperate glaciers (Winkler and Hagedorn, 1999; Curry et al., 2006): tens of meters high (up to ca. 200 m right from the glacier terminus; **Fig. 2**) and consisting of multiple stacked till units over-consolidated by basal accretion during successive advances (e.g. Lukas et al., 2012). The most prominent lateral moraine of MdG is located on the orographic right side, whereas deposits are almost absent from the left side of the valley in this region (**Fig. 2**). The outermost frontal moraine ridges located in the main valley floor are of late-LIA ages (Wetter, 1987; Nussbaumer et al., 2007). In the investigated sector, only the erosion edge is present in lateral position indicating that *superposition* (*sensu* Röthlisberger and Schneebeli, 1979) may have prevailed here, or that the latest deposited ridges have disappeared due to erosion. Two main sectors with subfossil wood outcrops were studied. The MOTT sector (right from the Rochers des Mottets roches moutonnées area) extends from ca. 1460 to 1700 m a.s.l. and corresponds to the RLM part located downstream of the present-day glacier terminus; the MDG sector extends from ca. 1700 to 1910 m a.s.l. and corresponds to the upstream sector, facing Montenvers (**Fig. 2**). The treeline above the study site roughly follows the 2100 m a.s.l. contour line. The timberline is composed of a monospecific multicentennial *Pinus cembra* stand in the cliffs above MDG sector, mixed with *Larix decidua* northward above MOTT sector.

Direct measurement of MdG frontal variations extends back to 1878 AD. This record indicates an overall retreat of 1.17 km until 2010, and three periods of readvance culminating in 1896 (+ 174 m), 1931 (+ 237 m) and 1995 (+ 143 m) (Reynaud and Vincent, 2000; C. Vincent, pers. com., 2011). The total retreat from LIA maxima positions amounts to 2.47 km. MdG has the longest reaction time among the northward flowing MBM glaciers. Its front readvances 11-14 yrs after nearby and most reactive (ca. 2-3 yrs) Glacier des Bossons (Martin, 1977; Reynaud, 1993; Nussbaumer and Zümbuhl, 2012). MdG dendro-reaction time (*sensu* Pelfini et al., 1997) has been fixed to 13 yrs over the 1878-2008 AD period by cross-correlation with a living *Pinus cembra* chronology distant from 6 km (Le Roy, 2012). Calculation of the response time according to the Jóhannesson et al. (1989)'s formula give ca. 40 yrs, whereas the analytical length response time has been fixed to 56 yrs by Klok and Oerlemans (2003). Note that these calculations do not take into account real-world topographical features. As a whole, these data indicate a glacier able to respond to decadal-scale cold events within an advance/retreat secular trend (Reynaud and Vincent, 2000; Nussbaumer et al., 2007).

3. Material and methods

3.1. Sampling procedure

Fieldwork extended over four seasons between 2009 and 2012. Sections of the lateral moraine were surveyed from the opposite valley side with a telescope (×30 to ×70 magnification) to locate the wood outcrops. Access was achieved both from the moraine crest, rappelling down the proximal face, and from its base, climbing up the gullies to reach the lowest till exposures.

Tree remains embedded-in-till appear most often as part of wood layers traceable over a few meters to tens of meters, some which may contain tens of debris ranging from centimetric fragments to logs several meters long and 80 cm in diameter. More rarely they come as isolated findings. Some of these woody layers are in contact with stratigraphical discontinuities such as paleosol, debris-rich litter horizons or fluvioglacial deposits (stratified gravels and sands). A single stump has been found unequivocally *in situ*, rooted in till material. Because of the difficulties to interpret ^{14}C dating of paleosol, priority was given to dendrochronological sampling. Some branches were also sampled in litter layers for radiocarbon dating. Additionally, the talus slope was carefully inspected. An exhaustive sampling of all subfossil-look tree remains lying on surface, or partly buried by colluviums, with long enough dendro-series (> ca. 60 rings) was carried out. Closely-spaced surveys conducted during each field seasons have permitted to determine with confidence from which woody layers in the till some reworked samples of the talus were coming from (e.g. **Fig. S4C**).

Several disks were cut from each log and fragment with a chainsaw. The best preserved parts of the trunks were sampled (e.g. in the vicinity of branch incipient for the eroded logs) to get the longest dendro-series. Scattered patchy bark remains were sampled additionally to provide a closest estimate for the tree death-date.

The moraine wood sample locations were surveyed with a TOPCON total station (accuracy < 1 m), and talus detrital woods with a GARMIN handheld GPS (accuracy ± 5 m). The altitude of the moraine erosion edge was recorded right from each subfossil wood sector. Their position is thus given in term of vertical distance to the moraine erosion edge.

3.2. Preparation and dendro-analysis

All sections were air-dried and sanded with progressively finer paper. The entire surface was polished to identify the longest and undisturbed measure paths. This procedure allows tracking rings over the whole circumference, and thus easier identification of missing rings. The narrowest rings sectors were prepared with razorblade and chalk powder or water to enhance rings boundaries definition. Ring-width measurements were recorded to the nearest 0.01 mm using a LINTAB 5 device associated to the TSAP software package (Rinntech, 2005). At least 3 radii were measured per sample and up to ca. 15 in the case of complex paths and/or poorly preserved samples. Radii were then crossdated according to standard dendrochronological procedures and averaged to produce mean individual series. Floating chronologies were built through crossdating of the individual series. The synchronization relies on statistical tests including the *Gleichläufigkeit* (Glk) and modified *t*-values (Baillie and Pilcher, 1973) computed in TSAP, as well as the visual inspection of curves fitting on screen. Samples species were determined under microscope according to anatomical keys (e.g. Schweingruber, 1990).

Moraine subfossil woods exhibit most of the time biological and mechanical alterations (Schweingruber, 2007). Rings were counted but not measured in the altered sectors, and added at the end of the measured series to provide a closer tree death-date estimate. Peripheral rings' counting was conservative to account for possible mis-interpretation. Therefore, a minimum tree lifespan (MTL) was estimated ending, most of the time, with a *terminus post quem* for tree-death, hereafter called *virtual* death-date and indicated by a "+". As sapwood identification is not possible with subfossil *Pinus cembra*, the quantification of missing external rings due to abrasion is tricky. A qualitative confidence level for the dendro-date is thus proposed, based on the sample preservation and the reliability of the counting (Tab. 1). It should be noted that the presence of bark or of the last ring (i.e. the so-called waney edge) does not always mean a yearly resolution for the tree death, as outermost rings may not be countable. A pith-offset estimate (PO) was carried out when the inner part of a sample was missing. The number of missing years was estimated through comparison with a Regional Growth Curve build from 335 *Pinus cembra* individual series sampled in the Central French Alps (Briançonnais area, ca. 120 km south of MBM; J-L. Edouard, unpublished data).

In sectors exhibiting a high density of subfossil wood remains and very large trunks, an effort was made to identify the fragments that belonged originally to the same tree (Tegel et al., 2012; Pichler et al., 2013). The proposed groupings rely on: (i) topographical field evidence, (ii) growth parameters (growth level and trend, PO, end-series date), and (iii)

crossdating values, for which conservative empirical thresholds were fixed (i.e. that mimic average intra-tree radii correlation). The highest crossdating value between two definitely different MdG trees, as well as the highest observed crossdating value between MdG and nearby Glacier d'Argentière subfossil samples both coincide ($t_{BP} \sim 10.5$). This threshold was thus used as lower limit for the groupings, although far lower values could characterize for instance samples from different heights on a single stem. All selected radii were then averaged as *single tree* series. In case some groupings were not identified this doesn't affect ages assigned to glacier advance which are based on the youngest age from each stratigraphically-defined layer.

3.3. Absolute dating

As a first step, radiocarbon dating was carried out on some samples to anchor floating chronologies in time and on some other samples difficult to date by dendrochronology. The radiocarbon samples include 5 to 15 rings and were taken after dendrochronological analysis, in order to know precisely their position in the dendro-series (Tab. 1). Measurements were carried out at the French LMC14 facility in Saclay (Cottereau et al., 2007) and at Beta Analytic Inc. (USA). Dating were calibrated with the CALIB 6.0 program (Stuiver et al., 2011) using INTCAL09 (Reimer et al., 2009). Dating results for samples only constrained by ^{14}C dating are reported by (i) the weighted average of the probability distribution function (Telford et al., 2004) to which the distance to the outermost counted ring was added; and (ii) the 2-sigma calibration range in brackets.

As no multi-millennial absolutely dated dendrochronological reference curve yet exists for the French Alps (see Edouard et al., 2002 and Edouard and Thomas, 2008 for an overview of existing data in this region) our resulting floating chronologies and single tree series were crossdated with the Eastern Alpine Conifer Chronology (EACC; Nicolussi et al., 2009). This chronology is based on living, dry-dead and subfossil mostly *Pinus cembra* (82%) wood sampled at the timberline (ca. 2000-2400 m a.s.l.) in the western Austrian massifs (ca. 350 km east of MBM; **Fig. 1**). In this paper, all dating results are reported according a time scale which includes a "year 0" at the beginning of the Common Era (dates of Common Era are labelled AD). Consequently, the true historical date of an event before this "year 0" is one year earlier than those reported hereafter (dates before Common Era are labelled BC). For instance, the reported dendro-date for the sample MDG.T120 is 1620 BC, but its death occurred in the calendar year 1621 BC.

3.4. Deriving an altitudinal glacier variations curve on its lateral margin

To constrain Neoglacial variations, altitudes of layers containing subfossil tree remains were compared with known altitudes of the MdG surface during the 20th century derived from field surveys (Reynaud and Vincent, 2000). In addition, profiles across the glacier through the moraine sampling sites were computed from digital elevation models (DEMs) obtained from old maps and photogrammetric surveys. The value used was the mean glacier surface altitude on its right margin. Analogues for the most extended Neoglacial glacier positions were not found during the 20th century and were thus estimated from the earliest photographs of the site dating back to the second half of the 19th century (Nussbaumer et al., 2007).

Fig. 3

Tab. 1

4. Results

4.1. Dendro-dating

Dendrochronological measurements were carried out on 205 samples from which 180 (88%) have been absolutely dated. The robustness of the MdG *Pinus cembra* series crossdating against EACC confirms a strong common signal across the Alps (Nicolussi et al., 2009). This high crossdating efficiency was made possible because of the low specific richness observed at MdG. Tree species determination indicates that 93% of the samples belong to *Pinus cembra* L. Other recorded taxa are *Acer* sp., *Larix decidua* Mill and *Picea abies* (L.) Karst (Tab. 1). Among dated series, the 10 samples from BAY moraine crest site are dry-dead fallen logs from the last millennium, and the 10 samples from moraine Site 7 were dated from the 20th century (see **Fig. 2** for the location and the Supplementary Materials for the description of the sites). All remaining moraine subfossil samples series were then grouped into 118 *single trees* series (as described in section 3.2). Additionally, 28 radiocarbon dates were determined (Tab. 1). Among these, 10 samples (including five twigs) are only constrained by radiocarbon dating.

Fig. 3 presents all dated subfossil samples – both with dendrochronology and radiocarbon (except the twigs) – together with the dry-dead samples from BAY site and the 20th century samples from Site 7. The clustering of the subfossil samples allowed the development of five mean ring-width chronologies covering the last four millennia with some minor gaps: from 2027 to 1544 BC, 1492 to 608 BC, 23 BC to 522 AD, 523 to 1339 AD and 1396 to 1854 AD. The 600 BC-0 period stands out by the relative lack of available subfossil wood remains as only one sample was recovered. MTL (including PO estimate) range for subfossil woods (except the 20th century samples) is comprised between 72+ and 487+ yr, with a mean of 232±91 yr. Mean ring-width (MRW) is 0.92±0.49 mm yr^{-1}. Average MTL and MRW are displayed in **Fig. 3** for each chronology. The main phases of tree germination and burial are reported on **Fig. 3D** to get an overview of stand dynamics – partly related to glacier behaviour (see section 5.1) – over the last 4 ka.

4.2. Geolocation

Spatial data acquired during the field surveys combined with the dating of both the embedded-in-till samples and the detrital samples reveal marked patterns. The results for the MDG sector are presented on **Fig. 4**. Wood outcrops from each time period are clearly distinct and there is a gradient regarding the age of the outcrops. Oldest samples were found only at the most upstream location (Sites 10 and 11) then, ages are getting younger downstream to the medieval period (Sites 5 and 6). Moreover, it is obvious from **Fig. 4** that the detrital samples are found right from outcrops of the same age – some of which have been sampled – which facilitates assigning some detrital samples to known layers from the moraine. A complete description of moraine wood outcrops and dating is given in the Supplementary Materials.

Fig. 4

5. Interpretation

5.1. Extracting past glacier variability from subfossil logs

Wood found within glacier forefield must be interpreted with respect to the initial growth location (Ryder and Thompson, 1986). At MdG, field evidence shows that few subfossil tree remains could be unambiguously considered *in situ*, i.e. *grown at finding place*. Such logs are interpreted as directly related to an advance of MdG. However, two other origins of the wood material has to be considered here: trees could have grown at other sites of the RLM than the finding place (i.e. at bedrock outcrops or stabilized moraine ridges) but were killed, transported and deposited during a glacier advance; or could have fallen from surrounding slopes and were deposited either (i) on a former moraine crest, (ii) on a former moraine proximal slope or (iii) on the glacier – prior to burial during a subsequent glacier advance.

In situ tree growth on a moraine ridge is proved for instance by the situation of the BAY01 stump (Site 6; **Fig. S3B**). Growth positions on a bedrock outcrop can be assumed, e.g. for many of the logs found at Sites 9, 10 and 11 (**Fig. 2**; **Fig. 4**; **Fig. S4-S5**). Such bedrock outcrops in the RLM were probably re-colonized during periods of glacier retreat and lateral moraine erosion. Trees from such growth sites killed during advances of MdG were deposited at other parts of the moraine as suggested by the high density of subfossil material in directly downstream locations (e.g. Site 9; **Fig. S4A**). Such a scenario involving tree recolonization of moraine proximal slopes has also been discussed at the Lower Grindelwald Glacier (Holzhauser and Zümbuhl, 1996). Therefore, these sites could have recorded glacier advances below the level of paleo-moraine crests. Finally, forests above finding places could have been a third source of origin for MdG logs. As the slope immediately above the RLM is almost entirely covered with trees and delivers dry-dead wood material to the moraine crest (BAY site; **Fig. S5F**) and the glacier surface, it can be assumed that analogue processes were also active in the past.

Dendrochronological analyses carried out on ten dry-dead logs lying on the present moraine crests at MdG and nearby Trient Glacier roughly suggest that bark and waney edge are preserved for ca. 10 yr and ca. 30 yr from the tree death, respectively (**Fig. 3B**). On the other hand, wood remains can be preserved subaerially up to several centuries in this environment before rotting away, as shown by samples from BAY site (**Fig. 3B**; **Fig. S5F**). These observations suggest that the degree of preservation of outermost rings indicates the time elapsed between the death of the tree and its burial. A sample with bark or waney edge over most of its surface resulted from a rapid burial and a short transport distance. It is thus interpreted as virtually *in situ* as it records a glacier position through burial with a sub-decadal temporal precision. On the contrary, a long exposition or a reworking is inferred when outermost part is shredded or heavily abraded and incrusted with gravels. Large

368 accumulations of eroded woody remains in contact with a paleo-surface like layer 2 at Site 6
369 (L2/S6; **Fig. S3D**) are thus interpreted as avalanched/dry-dead fallen trees on a former
370 moraine crest, resulting in differential aerobic decay.
371
372 **Fig. 5**
373
374 Although the link between glacier activity and tree death is not always straightforward
375 (particularly concerning the highly weathered fragments), the youngest dates in each defined
376 stratigraphical layers were considered as maximum ages for the till deposition that buried the
377 layers (Ryder and Thompson, 1986; Reyes and Clague, 2004; Koch et al., 2007). Detrital
378 woods sampled on the talus slope at the foot of the RLM have generally fallen from
379 contemporaneous strata sampled in the same sector (**Fig. 4; Fig. S4C**). Therefore, in some
380 cases (e.g. detrital samples slightly younger than embedded-in-till samples) they were used to
381 complement the information given by the woods sampled into the RLM. Maximum limiting
382 ages for MdG advance are reported on **Fig. 5** as well as correlation between the dated organic
383 levels.
384 The synthesis of MdG glacier surface variations over the last 4 ka determined from the
385 dated moraine sites is presented in **Fig. 6**. Basic principles followed to constrain glacier
386 variations from the subfossil wood record are those used elsewhere (e.g. Holzhauser, 2009;
387 2010; Holzhauser et al., 2005). However, given that the woods are not all *in situ* and their
388 origin not always known, we took into account these uncertainties in our representation.
389 When evidences of a paleo-moraine crest are found close to the woods (paleosol, laterally-
390 extensive and debris-rich layer, oxidized horizon), strata are represented by the youngest and
391 oldest tree death-dates. This interval corresponds to a period of wood accumulation on a
392 former moraine surface without till deposition. Oldest germination date from trees 'virtually
393 *in situ'* or 'of unknown original location' (either from within the glacier forefield or fallen
394 from the slope) provides evidence for a 'probable' or 'possible' glacier absence from the
395 corresponding level, respectively (**Fig. 6**).
396 The magnitude of glacier advances cannot easily be deduced from the vertical spacing of
397 dated wood horizons within lateral moraines (Kirkbride and Winkler, 2012). Yet we still use
398 this spacing as a first order estimate for the Neoglacial advances reconstructed here. Finally,
399 while our record represents thickness variations right from the subfossil wood layers, related

length variations can be assumed as shown by the long time series of direct topographic measurements available (Reynaud and Vincent, 2000).

The vertical scale used in **Fig. 5** is the vertical distance to the moraine erosion edge (simplified here as moraine crest). However, this scale is not relevant when the relative distance to the crest is not uniform along the entire forefield for a given advance. This is the case when two distant sites marking a medium-sized advance are correlated (e.g. the advance around 600 BC; see **Fig. 5**). Relative extents with respect to known historical altitude of MdG surface were thus used in **Fig. 6** to provide an homogeneous scale for all periods of advances.

Fig. 6

5.2. Subfossil wood-inferred Neoglacial history of MdG

The first advance dated at MdG occurred during the **Löbben period** (ca. 1900-1450 BC – 3850-3400 BP; Patzelt and Bortenschlager, 1973). MdG has exceeded the 1993 AD level from 1544+ BC as shown by the tree MDG119 sampled on the talus slope but which previously belong to L3/S10 (**Fig. S5D**). Other well-preserved logs show death in 1610 BC (MDG.T120), 1581 BC (MDG.T45), 1581+ BC (MDG5-01) and 1570+ (MDG.T117-118), which indicate that this advance spanned probably the first half of the 16th century BC. It is not possible to say if clustered virtual death-dates of detrital samples from the prior century between 1655+ BC and 1620+ BC indicate a previous burial episode during the second half of the 17th century BC, or if a significant part of outermost rings is lacking on these samples – as none of them exhibit waney edge (except MDG.T47_G dated to 1655+ BC – not an exact death-date but a close estimate; **Fig. 3A and Tab. 1 caption**). Maximum level of the glacier surface reached during the Löbben advance is not accurately known but could correspond to the 1950 AD level (altitude of L2/S9; **Fig. S4C**) or even to the 1939 AD level (altitude of L1/S10; **Fig. S5B**).

Death-date of five detrital samples broadly cluster around 1200 BC (1230+ BC to 1105+ BC). They could record a gradual burial episode marking an advance for which the vertical extent is not known. However, as evidence of bedrock outcrop recolonization by trees is proposed for L3/S9 from the 14th or 13th century BC, this **Late Bronze Age advance** must necessarily have been weaker than the 1993 AD level. We have not included highly decayed

MDG.T103 to this group as its death estimate at 1295+ BC should reflect an exposition in surface before being embedded during the Late Bronze Age Advance.

During the **Göschenen I period** (GI, ca. 1000-400 BC – 2950-2350 BP; Zoller et al., 1966) several advances of MdG can be documented. A maximum age for the first advance that buried trees is 962+ BC based on dated samples from L3/S9 (**Fig. S4D**) – or 937+ BC if we retain detrital samples. It roughly corresponds to the 1993 AD glacier surface level. Dated samples from L2 of the same site indicate that during the whole 10th century BC trees were growing higher up on the bedrock outcrop. This 10th century BC advance may has thus reached and exceeded the 1960-1988 AD level – but not the 1950 AD level – otherwise contemporary L2 trees would have already been killed at that time. The slightly 'too old' age obtained for the *in situ* stump MDG5-04 (L2/S10; **Fig. S5C**) at 1037 cal. BC (1131-978 cal. BC) does not allow to state whether its death can be linked to the glacier activity. It can have died and remained in standing position up to its burial during the 10th century BC advance. The large logs from L2/S9 (**Fig. S4C/E**), indicating a second GI-advance, show clustered death-dates (802 BC, 780+ BC and 777 BC). This could mean that the rise of the ice margin has spanned at least two decades. At that time the glacier exceeded the 1950 AD level and could have reached the 1939 AD level (altitude of L1/S10). The samples from L1/S9 (**Fig. S4B**) were probably buried during the same advance as shown by a virtual death-date based on wiggle-matching around 813 cal. BC (890-798 cal. BC). The last advance recorded during GI probably peaked at the end of the 7th century BC, as indicated by samples from both Site 2 and 10. The best preserved sample (MDG5-03; **Fig. S5B**) indicates a burial shortly after 608+ BC. This advance has probably exceeded the 1905 AD level and could even have peaked above the 1890 AD level (ca. 1870 AD level) as indicated by the altitude of L1/S3 and L3/S6. The paleo-surface upon which the paleosol found in contact with MOTT06 at Site 3 (**Fig. S1B**) has developed could thus have been deposited at that time.

The **Late Iron Age/Early Roman Era** is the most weakly represented time period in the MdG subfossil tree-ring record (**Fig. 3A**). Only one detrital sample has been dated from that period (171+ BC) so far and thereby can not be firmly linked to a glacier burial episode.

Robust evidences for a first advance during the **Göschenen II period** (GII, ca. 200-850 AD – 1750-1100 BP) is given by the virtually *in situ* and waney edge-bearing log MOTT01 (-82 m) dated to 312 AD and the fragments MOTT02 (-75 m) dated to 287+ AD and MOTT11 (-50 m) dated to 337 AD – all recording the rising of the ice margin during this event at Site 3 (**Fig. S1**). The glacier has thus exceeded the 1946 AD level as early as the beginning of the 3rd century AD (MOTT01; **Fig. S1C**). The stratigraphical discontinuity observed near MOTT11

466 sampling site (L3/S3) as organic silt deposition could indicate that the advance has peaked at
467 ca. 337 AD between the 1939 and 1905 AD levels. However, dating of MOTT13 (312+ AD)
468 found 30 m below the LIA moraine crest (i.e. 20 m above MOTT11), near layers thought to
469 have been buried during the 6th century AD, doesn't fit with this scheme (**Fig. S1**). It could be
470 explained either by (i) the lack of a large number of outer rings on sample MOTT13 or (ii)
471 that the first GII advance peaked effectively at this level (ca. 1890 AD level) sometimes
472 around the mid-fourth century AD. After this first GII advance, samples at Site 8 provide
473 evidence for a lowering of the glacier surface below the 1993 AD level around ca. 400+ / 402
474 AD. However, this retreat may also have occurred later (scenario ① and ② on **Fig. 6**; see the
475 Supplementary Materials and section 6.5 for explanations). Renewed progression of MdG can
476 be evidenced by tree death-dates in the late-fifth/early-sixth century AD at Site 3 (MOTT05,
477 485+ AD), Site 4 (MOTT.T06, 491+ AD) and a detrital log (MDG.T90, 525+ AD) that can be
478 linked to the L3/S6 based on its sampling location. However, as none of these trees are *in situ*,
479 the presence of the glacier can not be unambiguously proven at this level (L2/S3; ca. -28 m) at
480 the beginning of the 6th century. Most reliable evidences for the GII maximum come from Site
481 3 and Site 6 where two wood fragments (MOTT06 and MDG1-16), both located 24 m below
482 the crest, have yielded series that crossdate and give death-dates at 603 and 606+ AD,
483 respectively. The former sample was lying in contact with a paleosol (**Fig. S1B**) that could
484 correspond to the paleo-moraine crest deposited during either the last GI advance (ca. 600
485 BC) or the first GII advance (ca. 340 AD). The second sample had a standing position that
486 could not, however, be interpreted as an *in situ* position in the absence of excavation. This GII
487 maximum advance must have reached ca. 15 m below the LIA moraine crest, thus comparable
488 to the ca. 1860 AD glacier surface level.
489 A **High Medieval Advance (HMA)** is recognized at Site 5 (**Fig. S2**). The two dendro-
490 dated samples record the rising of the ice level during the 12th century, between 1120 AD and
491 1178 AD, as their preservation and location near palaeo-surfaces greatly minimizes growth
492 location uncertainties. This interpretation is reinforced by the five radiocarbon dates virtually
493 undistinguishable obtained on this vertical transect (**Fig. S2**). As this site is located at the
494 northern edge of MDG sub-sector 1 (see **Fig. 2**), the moraine palaeo-topography at the end of
495 the medieval period must have been subdued, enabling colonization of the proximal side by
496 trees. Germination of the virtually *in situ* MDG1-06 tree just prior to 866 AD could record the
497 length of the medieval glacier retreat with optimal conditions for tree colonization at that site.
498 Maximum vertical extent reached during this advance has exceeded the location of MDG1-09

499 at -19 m (ca. 1870 AD level) but could not have reached the level of L2 (-15 m) at nearby Site
500 6 – otherwise logs accumulation would have stopped at that time.
501 Following the HMA, **Early LIA** advances can be constrained at Site 6 (**Fig. S3**). The L2
502 layer has been buried after 1278+ AD. It could have happened after 1296 AD as shown by a
503 detrital wood with waney edge (MDG.T01) found slightly upstream, below the large bedrock
504 outcrop separating MDG sub-sectors 3 and 4. The L1 horizon has been buried after 1352+ AD
505 (MDG1-12; **Fig. S3E**). The temporal proximity of the different horizons marking HMA and
506 Early LIA events suggests a period with sustained high levels, interspersed with minor
507 lowerings of the glacier surface. The 14th century advance was the most important and
508 longest-lived of the three episodes, depositing the bulk of the 11 m-thick till upon which the
509 tree BAY01 has germinated around 1559 AD (**Fig. S3B**). As the maxima of the 17th and 19th
510 centuries (Nussbaumer et al., 2007) didn't affect BAY01 growth, this 14th century advance
511 could have been the LIA/Neoglacial most extensive advance at that site. An alternative
512 explanation involves the backwall retreat of the moraine edge that could have been important
513 since the end of the LIA. In this case, the 17th and 19th moraine ridges could have been
514 slightly higher but have not been preserved.
515 The **Late LIA** subfossil wood record is sparse at MdG. Few detrital woods have been
516 dated between the late 16th and early 19th centuries (**Fig. 3**). Moreover, it is not possible to
517 state whether they come from a buried layer already disappeared due to erosion, or if they
518 were dry-dead trees fallen from the rock cliff, laid some time on the moraine crest, before
519 they had fallen again due to the moraine backwall retreat. CHAP01 sample could represent a
520 tree crushed during the early 19th century advance (virtual death-date: 1821+ AD) and
521 reworked. If it's the case, this advance could have been the most extensive at that downstream
522 site (Site 1) since the Early LIA – as CHAP01 germination date is ca. 1575 AD.
523

524 # 6. Discussion

525

526 ## *6.1 Contribution to the Neoglacial glacier history of the Mont Blanc Massif*

527

528 The MdG chronology greatly improves the existing MBM Neoglacial chronology which
529 was exclusively based on ^{14}C dating until now (Corbel and Leroy Ladurie, 1963; Vivian,
530 1975; Bezinge and Vivian, 1976; Bezinge 1976; Orombelli and Porter, 1982; Bless, 1984;
531 Wetter, 1987; Deline and Orombelli, 2005). The MdG record starts at 3.6 ka and thus

532 confirms that the Löbben glacier advance period led to one of the first Neoglacial maxima in
533 the Alps (Patzelt and Bortenschlager, 1973; Bircher, 1982; Renner, 1982; Wipf, 2001;
534 Nicolussi and Patzelt, 2001; Ivy-Ochs et al., 2009; Schimmelpfennig et al., 2012).
535 Decreasing age downstream the RLM as recorded by the dated samples may represent in part
536 the multi-centennial trend of glacier advance increasing magnitude during the Neoglacial
537 from 3.6 ka (**Fig. 4**). An alternative explanation could involve differential deposition/erosion
538 of the till mantle. The thinner cover observed in the upstream sector located in the lee of Les
539 Echelets bedrock outcrop (**Fig. 2**) favouring the exposure of older sediments. Basal part of the
540 RLM was thus deposited during previous phases that remain to be precisely dated in MBM.
541 Only two sites have so far yielded older ages for an Early Neoglacial event – although their
542 chronological constraint remains imprecise. At Miage glacier, Deline and Orombelli (2005)
543 argued that damming of the valley by advancing glacier and subsequent start of glacio-
544 lacustrine sedimentation upstream of the dam occurred before ca. 4.8 ka. At Argentière
545 glacier, Bless (1984) has dated a wood associated with a paleosol located 130 m below the
546 crest at 3665±80 BP (2290-1780 cal. BC). This organic layer was stratigraphically distinct
547 from the two closely-spaced Löbben layers located 30 m higher up in the same profile and
548 dated to ca. 3300 BP (1860-1220 cal. BC).
549 Some sites sampled by Wetter (1987) at MdG correspond obviously to some of our dated
550 advances. This author reported dating of the GI advance at 2500±75 BP (795-415 cal. BC) for
551 woods located 25-30 m below the moraine crest, which is in line with the stratigraphical level
552 and age obtained for L1/S10 (**Fig. S5B**). On the other hand, dating at 1740±65 BP (125-430
553 cal AD) for an *in situ* stump located 30 m below the crest could indicate that the first GII
554 advance actually reached this level at Site 3, as discussed above (see section 5.2 and **Fig. S1**).
555 Since Wetter's survey, the lowering of the RLM local base level has partly uncovered its
556 lower part, which may explain he did not find any Löbben-aged tree remains.
557 The HMA and Early LIA (12^{th}-14^{th} centuries AD) had likely already been radiocarbon-
558 dated in the MBM. At Trient glacier, a paleosol located 12 m below the crest was dated to
559 825±55 BP (1045-1280 cal. AD) and record an advance larger than the 1896 AD level (Bless,
560 1984). At Miage glacier, a trunk fragment embedded-in-till 10 m below the crest has been
561 dated to 900±40 BP (1035-1215 cal. AD) (Deline, 1999). At MdG, an *in situ* trunk associated
562 with a well-developed paleosol located 10 m below the crest was dated to 730±70 BP (1165-
563 1400 cal AD) (Wetter, 1987).
564 The MdG 14^{th} century AD advance has likely been at least as important as the late LIA
565 advances of the 17^{th} and 19^{th} centuries as demonstrated by the *in situ* BAY01 stump growth

location (**Fig. S3B**). This assumption is supported elsewhere by the dating at 1315-1440 cal. AD of a paleosol buried by till deposit in outermost position with respect to the 1850 AD moraine at the Pré-de-Bard glacier (**Fig. 1**; Deline, 2002). This could indicate as well a Holocene maximum reached by this glacier during the 14th century advance.

Finally, our record also shed light on the regional vegetation history. The presence of *Pinus cembra* is attested since 8.9 ka in the nearby Fiz massif, with relatively high pollen percentages until 4.6 ka, then decreasing due to deforestation (**Fig. 1**, Survilly Bog; David, 2010). Our dendro record suggests a continuous presence of mature stands of this taxon during the last 4 ka on the Bayer slope above the RLM (**Fig. 2**). This is striking considering the scarcity of pure *Pinus cembra* stands in MBM nowadays and the widespread disappearance of this taxon in the western Alps after 5-4 ka (Ali et al., 2005; Finsinger and Tinner, 2007; Blarquez et al., 2010; David, 2010; Berthel et al., 2012). This site thus would have been a refugium for it because of the weak anthropogenic impact on this steep and remote rock slope.

6.2 Regional comparison of dendro-based glacier records

We compare here the dendro-based MdG record with other high-resolution glacier records from the alpine region: Great Aletsch (GA), Gorner (GO), Lower Grindelwald (LG) (Holzhauser and Zumbühl, 1996; Holzhauser, 1997; Holzhauser et al., 2005; Holzhauser, 2009; Holzhauser, 2010), Gepatschferner (GP) and Pasterze (PA) (Nicolussi and Patzelt, 2001), as well as some selected data constraining glacier variations during the Neoglacial (**Fig. 7**).

During the **Löbben period**, the last advance peaked after 1544+ BC at MdG – but no later than 1485-1460 BC as indicated by subsequent tree germination dates in the glacier forefield (**Fig. 3**); and after 1555 BC – but no later than 1500-1450 BC – at GP (Nicolussi and Patzelt, 2001). Similarly, at Allalin glacier the germination dates of trees will be killed during the first GI advance are recorded from 1458 BC (Röthlisberger et al., 1980; Bircher, 1982; Holzhauser, 2009). No clear evidence was found at MdG for a multi-phased Löbben advance period as proposed elsewhere in the Alps (e.g. Bircher, 1982; Renner, 1982; Bless, 1984; Wipf, 2001) or in the Coast Mountains of British Columbia (Osborn et al., 2013). In the Alps, the authors reported ^{14}C dating of several fossil soils attributed to this period (see review in Holzhauser, 2010). A first phase may have occurred in the 19th century BC as shown by a maximum age given by a detrital wood dendro-dated to 1851+ BC at Gorner glacier

(Holzhauser, 2010). This is in phase with a large germination event identified at MdG around 1822 BC±13 yrs (1σ, *n*=11; **Fig. 3D**). This cohort could record the forefield recolonization after a putative first Löbben advance. In the MdG RLM, woody layer from the Löbben period traceable at nearby Sites 10 and 11 contained trees that died between 1610 and 1544+ BC, but abundant detrital material could support assumption that this advance was already underway during the second half of the 17th century BC between ca. 1655+ BC and 1620+ BC (**Fig. 3A**). This was the case at GP where a first phase of glacier advance occurred between 1660 and 1626 BC which reached the 1930 AD level (Nicolussi and Patzelt, 2001). Detrital input into the Survilly peat bog also indicates two events constrained by a ^{14}C date at 3557 ± 82 cal. BP (ca. 1607 BC) sandwiched between the two detrital layers (**Fig. 7B**; David, 2010).

A burial episode ending the **Bronze Age Warm Period** could be proposed at MdG between ca. 1230+ BC and 1105+ BC (3180-3055 BP). As it is constrained only by detrital samples, maximum position reached during this advance is not known but should lie below the 1993 AD level. This advance has been recognized around 1200 BC at GP (ca. 1940 AD level), albeit also on the basis of a limited amount of detrital samples (Nicolussi and Patzelt, 2001). Similar dates came from GA where the glacier started to advance after the BWP around 1213/1211 BC.

The **GI** record is well represented at MdG. Stratigraphical evidence at Sites 9 and 10 shows that at least three discrete advances took place during this period, peaking after 962+ BC/937+ BC (2912/2887 BP), around 777 BC (2727 BP) and after 608+ BC (2558 BP). This behaviour is similar to LG and GP where more than one advance were recorded during the GI. At the same time, GA seem to have experienced a gradual and almost continuous frontal progression between ca. 1213 BC and 600 BC, punctuated by some still stands (Holzhauser et al., 2005; Holzhauser, 2009). Evidence for a 10th century BC advance exists also at Allalin glacier where it is constrained between 959 BC and 927 BC, when the glacier progression killed 400-500 yrs-old larch trees (Röthlisberger et al., 1980; Bircher, 1982; Holzhauser, 2009). Maximum extent reached by this reactive glacier corresponds to the ca. 1890 AD level – to be compared with the 2000 AD level exceeded by GA in 941 BC (Holzhauser, 2009). It should be noted that outside European Alps a very similar picture is described in Glacier Bay, Alaska. A radiocarbon-dated floating ring-width chronology from Geikie Inlet indicates that the glacier has started to progress in mature forest around 1259-1183 cal. BC (3209-3133 cal. BP) and that a major burial event occurred around 974-960 cal. BC (2924-2910 cal. BP). Germination of the trees killed during this advance occurred from 1650-1400 cal. BC (Wiles et al., 2011). Then, accurate kill-dates at 802, 780+ and 777 BC probably indicate MdG

progression into a forested slope during the second GI advance. At GP, the GI advance had two peaks, dated to shortly after 712 BC and a subsequent maximum reached around or after 637 BC. At that time it has exceeded the 1935 AD level, which is quite similar to MdG which has exceeded at least the 1905 AD level. Broadly speaking, the dates of GI maxima are very synchronous at MdG, GO and GA: around 608+, 602 and 600 BC, respectively. We found no evidence for other GI advances after 600 BC, despite high-stands (ca. 1920 AD level) were reported at Gefrorene Wand Kees (Eastern Alps) around 446+ BC (Nicolussi et al., 2006).

The **Late Iron Age-Early Roman Era** is the most weakly replicated period in the MdG dendro-record and could be interpreted either as: (i) a treeline lowering, that has been also observed in Eastern Alps but where it was mainly anthropogenically-induced (Nicolussi et al., 2005) – however, such an explanation for the MdG sample-gap is unlikely given continuous presence of trees at that site during the whole LIA; (ii) a period of sustained high glacier level which prevent the tree recolonization of the forefield – that is however not confirmed by LB record until 150 BC; or rather (iii) an extended withdrawal period which not allowed the burial – and therefore the preservation – of the trees. Nevertheless, the preservation of the lateral moraine (and therefore of older samples) on this multi-centennial time period requires that there have been some glacier advances which remain to be characterized more precisely.

The first **GII** advance was very restricted at GA (ca. 1982 AD level) whereas on more reactive glaciers this advance reached more advanced relative positions: between the 1939 and 1905 AD, or even the 1890 AD level (see Section 5.2 and 6.1) at MdG, and beyond the 1930 AD level at GP. Culmination of this advance yields very similar date at GP and MdG: just after 336 and 337 AD, respectively. Following that advance we propose a retreat centred on 400+/402 AD based on samples from Site 8 (the two retreat scenarios are discussed in the light of paleoclimatic proxies in section 6.5). It may be noted that a possible retreat centred on 370 AD has also been proposed at GA (Holzhauser et al., 2005; H. Holzhauser pers. com., 2014). The main discrepancy in the timing of Neoglacial events at an Alpine scale comes from the second part of the GII period. The MdG chronology seems to agree with large Swiss glaciers records (GA and GO; Holzhauser et al., 2005; Holzhauser, 2009; Holzhauser, 2010), i.e. probably advanced positions already reached at the beginning of the 6th century and near Holocene maximum reached at the beginning of the 7th century. At GA, the advance is well constrained between 430 AD (1970 AD level) and 590 AD (1870 AD level), with the highest progression rate from 532 AD onwards (Holzhauser, 2009), leading to a near-Holocene maximum ca. 630 AD. Similar dates come from other Swiss glaciers: Ried glacier advanced around 525 AD, Zmutt glacier crushed a 400 yr-old larch tree in 580 AD, and LG crushed

668 trees between 527 and 595 AD (Röthlisberger, 1976; Röthlisberger et al., 1980; Holzhauser,
669 1985; Holzhauser and Zumbühl, 1996; Holzhauser, 2009) – although the most advanced
670 position achieved at that time by these three glaciers is not precisely known (Holzhauser,
671 2010). On the other hand, evidences from PA, GP and Suldenferner (Eastern Alps) indicate
672 that the first millennium AD maximum extent was reached at the beginning of the 9th century
673 AD (809-834 AD) – with extents exceeding that of 1925, 1920 and 1880 AD, respectively –
674 and that no maxima occurred at the turn of the 6th-7th century AD (Nicolussi and Patzelt,
675 2001; Nicolussi et al., 2006; McCormick et al., 2012). The advance in the early 9th century is
676 also dated on western-Alpine Swiss glaciers among which LG is the best constrained with
677 dendro-dates spanning 820 to 836 AD (Holzhauser and Zumbühl, 1996; 2003). In the MBM,
678 sparse proofs of a prominent 9th century advance include ^{14}C and dendro-dating of logs in
679 stratigraphic positions at Brenva and Argentière glaciers (Orombelli and Porter, 1982; Le
680 Roy, 2012). Pending new data, a working hypothesis could be that the '600 AD advance' has
681 been stronger in the western part of the Alps – or that more evidences of it have been
682 preserved – leading to the 'First Millennium maximum'. In contrast, evidences for an inverted
683 hierarchy concerning the '830 AD advance' are unequivocal: this advance has been the
684 strongest from the first millennium in the Eastern Alps. One can note that MdG behaviour
685 during the GII period also agree with some North Western North American glaciers. A two-
686 step advance has been described and dated at numerous locations with maxima reached
687 around 100-250 cal. AD (1850-1700 cal. BP) and 470-500 cal. AD (1480-1450 cal. BP),
688 separated by a small retreat (Jackson et al., 2008; Hoffmann and Smith, 2013). However, at
689 other sites only a continuous advance peaking during the 7th or early 8th century AD is
690 documented (Reyes et al., 2006; Barclay et al., 2009; 2013; Johnson and Smith, 2012).
691 Finally, the MdG record shows unequivocally that a large advance (**HMA**) interrupted the
692 MWP during the 12th century, peaking around 1178 AD. In the Alps, other sites where this
693 advance was dendro-dated include Ferpècle, LG, Zinal (ca. 1890 AD level), GP (>1930 AD
694 level), GO (ca. 1954 level) at 1125, 1137, 1159, 1172 and 1186 AD, respectively (Haas, 1978;
695 Holzhauser, 1985; Röthlisberger et al., 1980; Nicolussi and Patzelt, 2001; Holzhauser, 2010).
696 At GA, a maximum age of 1100 AD was determined for this advance, corresponding to the
697 1920 AD level. Advances at that time were also demonstrated recently in a number of
698 Northern Hemisphere locations (see Koch and Clague, 2011). Early LIA advances peaked
699 around 1296 AD and after 1352+ AD at MdG – the later likely reached Holocene maxima.
700 The 14th century maximum is comparable to the LG, GA and GO first LIA maxima reached
701 around 1338, 1369 and 1385, respectively (Holzhauser et al., 2005). Nonetheless, the 14th

century glacier highstand seems to be less extended in the eastern Alps. GP has exceeded the 1870 AD level in 1284 AD in good agreement with MdG, and again in 1462 AD – without evidence for reaching a LIA maximum extent in the 14th century. Similarly, PA remained smaller than the 1890 AD extent around 1350 AD (Nicolussi and Patzelt, 2001).

Fig. 7

6.3 Role of glacier response time

Alpine glacier chronologies show in general a high level of similarity in the timing of Neoglacial events (**Fig. 7**). Major differences between the records arise from the relative magnitude of the different advances. Despite the partial nature of terrestrial Neoglacial glacier records which lack continuity, those differences – particularly visible for the second-order advances – could be explained in the light of the respective glacier response times. GA and GO have a reaction time of ca. 25 yrs (Müller, 1988) and a response time around 80 yrs according to the Jóhannesson et al. (1989)'s formula. These values are twice those proposed for MdG. It follows that during the first GII advance, GA reached the 1982 AD level but did not exceed with certainty the 1970 AD level, whether the MdG advance peaked between the 1939 and 1905 AD levels. During the 12th century AD advance, GO reached the 1949 AD level but didn't exceed with certainty the 1940 AD level, whether MdG reached at least the 1870 AD level. In contrast, MdG and LG seems react to climate with quite similar time-lags. Published analytical length response times are 52 yrs for LG and 56 yrs for MdG (Klok and Oerlemans, 2003); as 22 yrs and 40 yrs, respectively, with the Jóhannesson et al. (1989)'s formula. Numerical modelling has yields a length response time in the range 34-45 yrs for LG (Schmeits and Oerlemans, 1997). Furthermore, the correlation of their length variations over the last 500 yrs reveals the best fit when setting a 1-yr lead for MdG relative to LG (Nussbaumer et al., 2011). However, full comparison of the two records on the whole Neoglacial time period is prevented by the sediment deposition patterns at LG which does not allow proposing a magnitude scale for its advances prior to the LIA (H. Holzhauser, pers. com., 2014). GP seems also to have a similar response time as MdG as the Jóhannesson et al. (1989)'s formula yields ca. 26 years, taking into account present-day values of ablation at the terminus (M. Stocker-Waldhuber, pers. com., 2014). This is confirmed by the relative extent reached during most of the Neoglacial advances, quite similar to the levels reached by MdG

(e.g. during the GI maximum, the first GII advance and the 13th century AD advance; see section 6.2). Finally, it appears that PA has a much delayed response to climate as published length response time range from 62 yrs to 70-137 yrs according to analytical and numerical modelling attempts, respectively (Zuo and Oerlemans, 1997; Klok and Oerlemans, 2003). This is evidenced by its behaviour during the Löbben period or at the beginning of the LIA, when it was more retracted than most other alpine glaciers. Peat growth in the forefield indicate that the front was upstream of the present terminus between either, 1800 and 1550 BC, or 1940 and 1430 cal. BC (Nicolussi and Patzelt, 2001; Kellerer-Pirklbauer and Drescher-Schneider, 2009). Likewise, from the GII to the 17th century AD, it has never exceeded its 1890 AD level (Nicolussi and Patzelt, 2001). To summarize, we have seen based on the most robust evidences, that the different glacier behaviours are clearly reflected in the dendro-based Alpine Neoglacial glacier chronologies.

6.4 Comparison with regional lake sediment records

The newly established MdG glacier curve provide the opportunity to directly test assumptions made about the link between glacier variations in high catchment areas and rate and origin of sediment deposition in the subalpine Lake Le Bourget (LBo; **Fig. 1**) as MdG belongs to the sporadic watershed of the lake (Arnaud et al., 2005, 2012; Debret et al., 2010). Dendro-death dates providing maximum ages for MdG advances are reported in **Fig. 7** together with the titanium (Ti) content measured in core LDB04-1 which is a proxy for the terrigenous fraction brought by Rhône river flooding into LBo (Jacob et al., 2008; Arnaud et al., 2012). We also compare our results to the clastic record of proglacial Lake Bramant located in the Grandes Rousses massif (LBr; **Fig. 1**). This record has been interpreted as a proxy for glacier activity in the catchment (**Fig. 7F;** Guyard et al., 2013). Moreover, it is particularly sensitive to retreat phases as the lake catchment only includes the western diffluent part of the Saint Sorlin glacier. To get a broader overview at the North Atlantic scale we also depicted in **Fig. 7E** two glacier activity records based on lake sediments from Norway (Bakke et al., 2010; Vasskog et al., 2012).

A very significant excursion of the K/Ti ratio peaking between 1600 and 1400 BC in LBr record is highly consistent with our results. It encompasses the MdG advance that peaked after 1544+ BC, indicating that St Sorlin glacier was also in advanced position at that time. It may be noted that lake-based reconstructions show a maximum rather centred on 1440 BC (**Fig. 7E/F/H**), while there are already evidences of glacier forefields tree recolonization at

769 that time in the Alps (see section 6.2). This likely highlights the transfer time in the
770 sedimentary systems. After a retreat of Saint Sorlin glacier during the BWP, a strong rise
771 occurred from 900 BC which tightly corresponds to the first GII advance at MdG dated to
772 after 937+ BC. Sustained high values persisted then until 450 BC, which is consistent with
773 highstands mentioned in Austrian Alps at that time (see section 6.2). From the GII period, it is
774 noteworthy that almost every MdG advances correspond to a significant detrital peak in LBo.
775 This is particularly clear for the second GII advance dated to 802-777 BC at MdG, which
776 corresponds to a sharp rise in terrigenous flux peaking around 773 BC in LBo. Sustained
777 moderately high levels continue afterwards till around 622 BC. Then, evidence for two
778 distinct events during the Göschenen II period is unambiguous in both records. The first one
779 is dated to 337 AD at MdG, which corresponds to the Ti peak at ca. 342 AD in LBo. The
780 second event is constrained at MdG by two death-dates in 603 and 606+ AD, in good
781 agreement with a Ti peak around 586 AD in LBo. In contrast, anomalies of K/Ti from LBr
782 show only a single peak at that time between ca. 400 and 550 AD.
783 The HMA is well constrained at MdG by virtually *in situ* and waney edge-bearing woods
784 that indicate the rising of the ice margin during the 12th century, up to a culmination around
785 1178 AD (**Fig. S2**). This is in agreement with a short-lived but strong detrital peak around
786 1163 AD in LBo and a marked Ti excursion around 1170 AD in LBr. Again, the late 13th
787 century AD highstand at MdG followed by the first LIA maximum after 1352+ AD closely
788 corresponds to the lake records. The full sedimentological/erosional LIA conditions in both
789 lakes seem to begin in the late 13th century AD with a first maximum reached between 1290
790 and 1320 AD in LBo and a Ti peak centred on 1295 AD in LBr (**Fig. 7F/H**).
791 On the other hand, some moderate Ti peaks in LBo record (e.g. 150 to 100 BC), without
792 correspondence with known MdG advances, could result from anthropogenic action. The 400
793 BC-400 AD period has been for instance considered a period of anthropogenic-induced soil
794 erosion – hindering the climatic signal – from the Lake Anterne flood record (Giguet-Covex
795 et al., 2012). Nevertheless, further work on glacier chronology is needed as several evidences
796 could suggest an advance during the Roman period: (i) a single tree has been dated to the
797 early Roman Era (171+ BC) at MdG, insufficient to highlight a burial episode; (ii) a log
798 located 15 m below the moraine crest at nearby Argentière glacier has been dated to 68 cal.
799 BC (197-46 cal. BC; Le Roy, 2012); (iii) an advance has ever been proposed during the
800 Roman period around 50 BC at GP (Nicolussi and Patzelt, 2001 : 45); (iv) a prominent K/Ti
801 anomaly centred on 70 BC – of similar magnitude to the excursion recorded around 500 AD –

exists in the Lake Bramant record (**Fig. 7F**; Guyard et al., 2013); and (v) some Scandinavian glaciers are advancing at that time (**Fig. 7E**; Bakke et al., 2010).

Interestingly, the three Austre Okstindbreen (northern Norway) late Holocene maxima occurred synchronously with MdG and alpine glaciers (albeit slightly delayed in the lake record): between 650 and 760 AD, between 1150 and 1410 and between 1680 and 1900 AD (**Fig. 7E**; Bakke et al., 2010). These three maxima were preceded by a well-distinct advance peaking around 370 AD which can be linked to the first GII advance in the Alps (**Fig. 7A/B/C/E**). Overall, this means a high synchronicity between Scandinavian and Alpine glaciers at the multi-decadal scale during at least the last 2000 years.

Fig. 8

6.5 Climatic controls of western Alps glacier variations during the Neoglacial

Comparison of the MdG record with other high resolution glacier records from the Alps and other mid-latitudes areas reveal a high degree of similarity at a multi-decadal scale (**Fig. 7A-E**), calling for a strong common forcing. The sun is the main driver of Earth's climate system (e.g. Lockwood, 2012) and Holocene variations in solar activity could have modified the energy balance of the Earth through variations in total solar irradiance (TSI). Based on proxies correlation, many studies have thus claimed that solar input has paced Holocene climate (e.g. Bond et al., 2001; Magny, 2004; Magny et al., 2010; van Geel and Mauquoy, 2010) and was an important driver for glacier variations at different times-scales (Wiles et al, 2004; Hormes et al., 2006; Koch and Clague, 2006; Nussbaumer et al., 2011). Yet the magnitude of TSI changes during the Holocene remains very controversial (e.g. Shapiro et al., 2011; Steinhilber et al., 2009; 2012) and recent modelling efforts have shown that solar forcing probably had a minor effect on the Northern Hemisphere climate during the last millennium (Schurer et al., 2014). Similarly, Lüthi (2013) found no significant relationship between reconstructed ELA series and TSI for the last 1600 yrs in the Alps – except during the 1700-1950 AD period. Nevertheless, visual comparison of the MdG chronology with a TSI record show that most of the major Neoglacial advances tightly correspond to abrupt TSI drop, e.g. around 1500 BC, 1000 BC, 800 BC, 600 AD and 1275 AD (**Fig. 8A/B**).

The North Atlantic Oscillation (NAO) is the most prominent mode of atmospheric variability over the North Atlantic Ocean and Northwestern Europe (Wanner et al., 2001). It

has the strongest influence on winter climate. The NAO impact on Alpine climate is equivocal due to the situation of the chain at the transition between northern and southern Europe, characterized by opposite NAO patterns. In the Alps, the main control of glacier mass balance variability is summer temperature (Vincent et al., 2004), but precipitation become increasingly important to explain mass balance sensitivity in the western part of the range and close to its northern fringe (e.g. in MBM) – where climate is moister (Marzeion et al., 2012). Several studies have found an anti-correlation between western alpine glaciers length change or mass balance data and a NAO index at the decadal scale during the modern period (Six et al., 2001; Reichert et al., 2001; Imhof et al., 2012; Marzeion and Nesje, 2012; Guyard et al., 2013), while at more sheltered site no correlation was found, even with the winter mass balance (Thibert et al., 2013). From this, the NAO seems to partly control mass balance in the northwestern Alps – albeit to a lesser extent than for the more maritime Scandinavian glaciers. Comparison of the MdG chronology with a NAO reconstruction covering the whole Neoglacial shows that glacier advance seems to be associated with NAO negative phases or variable conditions – at least until the GII, and then during the second part of the LIA (**Fig. 8B**). Persistent positive mode just before and throughout the MWP suggests that another forcing was responsible for the HMA and Early LIA glacier advances.

Volcanic aerosols released during major explosive eruptions reflect and scatter solar radiation which results in Earth surface cooling (Robock, 2000). At Holocene scale, an above-average frequency of eruptions characterizes the last two millennia (Castellano et al., 2005). This forcing was found to be the cause for the onset of the LIA in the second half of the 13th century (Miller et al., 2012) owing to an exceptional cluster of high magnitude eruptive events between 1230 and 1275 AD (Gao et al., 2008). This is in phase with the high frequency of tree death-dates recorded at MdG during the 13th century AD (n=13; **Fig. 3**) – only surpassed in our record by the 1650-1550 BC time period (n=16). Apart from the LIA, the volcanic imprint is likely present in the temperature and glacier records during two others periods. After a "Löbben interstadial" peaking around 1730-1700 BC which is well marked both in paleo-temperature proxies and MdG subfossil trees replication (**Fig. 8E/F/H**), the coldest interval of the period spans ca. 1660 to 1500 BC with cold peaks centred on ca. 1625 BC and ca. 1530 BC (**Fig. 8F**). The first cold pulse is synchronous with the eruption of Thera (Santorini), radiocarbon-dated between 1660 and 1600 cal. BC (Friedrich et al., 2006), but which could more tightly corresponds to a growth depression centred on 1628-1627 BC in trees from several northern hemisphere locations (Baillie and Munroe, 1988; Grudd et al., 2000; Salzer and Hughes, 2007). Similarly, during the Göschenen II period, the so-called

"540 AD event" is also known to be an abrupt volcanic-induced cooling that spans a decade or so from 536 AD (Baillie, 2008; Larsen et al., 2008; Ferris et al., 2011). This cooling must have contributed to the 6th/early 7th century glacier advance, as GA show for instance the highest progression rates from the 530 AD decade. Direct influence of volcanism on climate is relatively short-lived but could be amplified when multiple events occur at short interval or through radiative cooling transfer to the ocean (e.g. Stenchikov et al., 2009). These reasons may explain the volcanic forcing has been substantially driven glacier advances on a decadal scale during the Neoglacial period.

It is likely that the major advances were caused by the interplay of several forcing like around 600 AD, in the 13th century AD and during the second part of the LIA. Overall, proposed MdG chronology appears broadly consistent with independent paleoclimatic evidences in terms of temperature reconstruction (**Fig. 8E/F**), which confirms that temperature, mainly from the warm season, was the main driver of MdG fluctuations during the Neoglacial. Nevertheless, our proposed withdrawal centred on 400 AD seems to conflict with available climatic reconstructions. This period was likely cold and humid (Büntgen et al., 2011), unfavorable to a rapid and marked glacial retreat as suggested in our scenario ① (Fig. 6). Other candidate periods for such a retreat, allowing the tongue to down waste to ca. the 1993 AD level, could be found either around 500 AD or between 850 and 1050 AD (scenario ②, Fig. 6) according to available paleoclimatic evidences.

7. Conclusion

We present here the first high-precision glacier chronology for the westernmost Alps, establishing a precise constraint on the Neoglacial events in this area. The geographical setting at MdG allowed a large sampling that permitted to highlight numerous burial episodes but the scarcity of formally *in situ* trees somewhat complicates the interpretation of the datings. Dendrochronologically-dated subfossil wood remains from the right lateral moraine have permitted to constrain 10 glacier advances between 1600 BC and 1400 AD. Culmination of these advances occurred: after 1544+ BC (3494 BP), after 1105+ BC (3055 BP), after 937+ BC (2887 BP), around 777 BC (2727 BP), after 608+ BC (2558 BP), around 337 AD (1613 BP), after 606+ AD (1344 BP), around 1178 AD (772 BP), around 1296 AD (654 BP) and after 1352+ AD (598 BP). Most of these advances could be tightly linked to Rhône river

flooding events into Lake Le Bourget, confirming this record as a valuable glacial erosion proxy.

The picture emerging from the MdG forefield is very consistent with other high resolution glacier variation curves from the European Alps and northwestern North America. It confirms a millennial trend of glacier growth that culminates during the LIA. Despite general agreement at regional scale, the major discrepancy between "western" and "eastern" available Alpine glacier records comes from the first millennium AD (Göschenen II period around 500-850 AD – 1450-1100 BP). More work is needed to determine if it could arise from a real paleoclimatic difference.

Ongoing sampling effort focusing on other MBM glaciers (especially Glacier d'Argentière and Glacier des Bossons) should yield additional data and improve this glacial chronology, particularly concerning several poorly documented periods at MdG like the Neoglacial onset around the so-called 4.2 ka event, the Roman Era and the Early Medieval Period (9th century AD).

Acknowledgements

MLR PhD project was funded by French Ministry of Higher Education and Research. Logistical and analytical support was provided by the French National Research Agency program *Pygmalion* (ANR BLAN07-2_204489). KN is supported by the Austrian Science Fund (I 1183-N19). We warmly acknowledge Ludovic Ravanel, Emmanuel Malet and Didier Simond for their invaluable help in the field, as Christian Vincent, Samuel Nussbaumer and Wolfgang Wetter for sharing personal data.

References

Ali A.A., Carcaillet C., Talon B., Roiron P., Terral J.-F., 2005. *Pinus cembra L.* (arolla pine), a common tree in the inner French Alps since the early Holocene and once extended above the present treeline: a synthesis based on charcoal data from soils and travertines. Journal of Biogeography 32, 1659–69.

Arnaud F., Revel-Rolland M., Chapron E., Desmet M., Tribovillard N., 2005. 7200 years of Rhône river flooding activity recorded in Lake Le Bourget: a high resolution sediment record of NW Alps hydrology. The Holocene 15, 420–428.

933 Arnaud F., Révillon S., Debret M., Revel M., Chapron E., Jacob J., Giguet-Covex C., Poulenard J.,
934 Magny M., 2012. Lake Bourget regional erosion patterns reconstruction reveals Holocene NW
935 European Alps soil evolution and paleohydrology. Quaternary Science Reviews 51, 81–92.
936 Baillie M.G.L., 2008. Proposed re-dating of the European ice core chronology by seven years prior to
937 the 7th century AD. Geophysical Research Letters 35, L15813, doi:10.1029/2008GL034755.
938 Baillie M.G.L., Pilcher J.R., 1973. A simple cross-dating program for tree-ring research. Tree-ring
939 Bulletin 33, 7–14.
940 Baillie M.G.L., Munro M.A.R., 1988. Irish tree rings, Santorini and volcanic dust veils. Nature 332,
941 344–346.
942 Bakke J., Dahl S.O., Paasche Ø., Simonsen J.R., Kvisvik B., Bakke K., Nesje A., 2010. A complete
943 record of Holocene glacier variability at Austre Okstindbreen, northern Norway: an integrated
944 approach. Quaternary Science Reviews 29, 1246–1262.
945 Barclay D.J., Wiles G.C., Calkin P.E., 2009. Tree-ring crossdates for a First Millennium AD advance
946 of Tebenkof Glacier, southern Alaska. Quaternary Research 71, 22-26.
947 Barclay D.J., Yager E.M., Graves J., Kloczko M., Calkin P.E., 2013. Late Holocene glacial history of
948 the Copper River Delta, coastal south-central Alaska, and controls on valley glacier fluctuations.
949 Quaternary Science Reviews 81, 74-89.
950 Beedle M.J., Menounos B., Luckman B.H., Wheate R., 2009. Annual push moraines as Climate
951 proxy. Geophysical Research Letters 36, 20, doi:10.1029/2009GL039533.
952 Berthel N., Schwörer C., Tinner W., 2012. Impact of Holocene climate changes on alpine and treeline
953 vegetation at Sanetsch Pass, Bernese Alps, Switzerland. Review of Palaeobotany and Palynology
954 174, 91–100.
955 Berthier E., Arnaud Y., Baratoux D., Vincent C., Rémy F., 2004. Recent rapid thinning of the Mer de
956 Glace glacier derived from satellite optical images. Geophysical Research Letters 31, 17, L17401
957 (doi: 10.1029/2004GL020706).
958 Berthier E., Vincent C., 2012. Relative contribution of surface mass balance and ice flux changes to
959 the accelerated thinning of the Mer de Glace (Alps) over 1979-2008. Journal of Glaciology 58,
960 209, 501–512.
961 Bezinge A., 1976. Troncs fossiles morainiques et climat de la période holocène en Europe. Bulletin de
962 la Murithienne 93, 93–111.
963 Bezinge A., Vivian R., 1976. Bilan de la section de glaciologie de la société Hydrotechnique de
964 France: sites sous glaciaires et climat de la période holocène en Europe. La Houille Blanche 6-7,
965 441–459.
966 Bircher W., 1982. Zur Gletscher- und Klimageschichte des Saastales: Glazialmorphologische und
967 dendroklimatologische Untersuchungen. Physische Geographie 9, Zürich.

968 Blarquez O., Carcaillet C., Bremond L., Mourier B.., Radakovitch O., 2010. Trees in the subalpine
969 belt since 11 700 cal. BP: Origin, expansion and alteration of the modern forest. The Holocene 20,
970 139–146.
971 Bless R., 1984. Beträge zur Spät- und Post-glazialen Geschichte der Gletscher im Nordöstlichen Mont
972 Blanc Gebiet. Physische Geographie 15, Zürich.
973 Boch R., Spötl C., 2011. Reconstructing palaeoprecipitation from an active cave flowstone. Journal of
974 Quaternary Science 26, 7, 675–687.
975 Bond G., Kromer B., Beer J., Muscheler R., Evans M.N., Showers W., Hoffmann S., Lotti-Bond R.,
976 Hajdas I., Bonani G., 2001. Persistent solar influence on North Atlantic climate during the
977 Holocene. Science 294, 2130–2136, doi:10.1126/science.1065680.
978 Büntgen U., Tegel W., 2011. European tree-ring data and the Medieval Climate Anomaly. PAGES 19,
979 14–15.
980 Büntgen U., Tegel W., Nicolussi K., McCormick M., Frank D., Trouet V., Kaplan J., Herzig F.,
981 Heussner U., Wanner H., Luterbacher J., Esper J., 2011. 2500 years of European climate
982 variability and human susceptibility. Science 331, 578–582.
983 Bussy F., von Raumer J.F., 1994. U-Pb geochronology of Palezoic magmatic events in the Mont Blanc
984 crystalline massif, Western Alps. Schweizerische Mineralogische und Petrographische
985 Mitteilungen 74, 514–515.
986 Bronk Ramsey C., van der Plicht H., Weninger B., 2001. "Wiggle Matching" Radiocarbon dates,
987 Radiocarbon 43, 2A, 381–389.
988 Castellano, E., Becagli, S., Hansson, M., Hutterli, M., Petit, J.R., Rampino, M.R., Severi, M.,
989 Steffensen, J.P., Traversi, R. and Udisti, R., 2005. Holocene volcanic history as recorded in the
990 sulphate stratigraphy of the European Project for Ice Coring in Antarctica Dome C (EDC96) ice
991 core. J. Geophys. Res., 110, D06114, doi: 10.1029/2004JB005259.
992 Cottereau E., Arnold M., Moreau C., Baqué D., Bavay D., Caffy I., Comby C., Dumoulin J-P., Hain
993 S., Perron M., Salomon J., Setti V., 2007. Artemis, the new ^{14}C AMS at LMC14 in Saclay, France.
994 Radiocarbon 49, 291–299.
995 Curry A.M., Cleasby V., Zukowskyj P., 2006. Paraglacial response of steep, sediment-mantled slopes
996 to post- 'Little Ice Age' glacier recession in the central Swiss Alps. Journal of Quaternary Science
997 21, 3, 211–225.
998 Dahl S.O., Bakke J., Lie Ø., Nesje A., 2003. Reconstruction of former glacier equilibrium-line
999 altitudes based on proglacial sites: an evaluation of approaches and selection of sites. Quaternary
1000 Science Reviews 22, 275–87.
1001 David, F., 1997. Holocene tree limit in the northern French Alps stomata and pollen evidence. Review
1002 of Paleobotany and Palynology 97, 227–237.
1003 David F., 2010. An example of the consequences of human activities on the evolution of subalpine
1004 landscapes, Comptes Rendus Palevol. 9, 5, 229–235.

1005 Davis P.T., Menounos B., Osborn G., 2009. Latest Pleistocene and Holocene alpine glacier
1006 fluctuations: a global perspective. Quaternary Sciences Reviews 28, 2021–2033.
1007 Debret M., Chapron E., Desmet M., Rolland-Revel M., Magand O., Trentesaux A., Bout-Roumazeille
1008 V., Nomade J., Arnaud F., 2010. North western Alps Holocene paleohydrology recorded by
1009 flooding activity in Lake Le Bourget. France. Quaternary Science Reviews 29, 2185–2200.
1010 Deline P., 1999. Les variations holocènes récentes du glacier du Miage (Val Veny, Val d'Aoste).
1011 Quaternaire 10, 1, 5–13.
1012 Deline P., 2002. Geomorphological study of rock avalanche and glacier interactions in the high alpine
1013 mountain: the south eastern side of the Mont Blanc massif (Valley of Aosta, Italy) [in french]
1014 Unpublished PhD thesis, Université de Savoie, 365 p.
1015 Deline P., 2005. Change in surface debris cover on Mont Blanc massif glaciers after the 'Little Ice
1016 Age' termination. The Holocene 15, 2, 302–309.
1017 Deline P., Orombelli G., 2005. Glacier fluctuations in the western Alps during the Neoglacial as
1018 indicated by the Miage morainic amphiteatre (Mont Blanc massif, Italy). Boreas 34, 456–467.
1019 Deline P., Gardent M., Kirkbride M.P., Le Roy M., Martin B., 2012. Geomorphology and dynamics of
1020 supraglacial debris covers in the Western Alps. *Geophysical Research Abstracts*, 14, EGU2012-
1021 10866.
1022 Denton G.H., Karlén W., 1973. Holocene climatic variations: their pattern and possible cause.
1023 Quaternary Research 3, 155–205.
1024 Edouard J-L., Guibal F., Nicault A., Rathgeber C., Tessier L., Thomas A., Wicha S., 2002. Arbres
1025 subfossiles (Pinus cembra, Pinus uncinata et Larix decidua) et évolution des forêts d'altitude dans
1026 les Alpes françaises au cours de l'Holocène. Approche dendrochronologique. *In* Richard H. et
1027 Vignot A. (Eds.) Actes du colloque international « Equilibre et rupture dans les écosystèmes
1028 depuis 20000 ans en Europe de l'Ouest : durabilité et mutation », Annales littéraires, 730. Série
1029 "Environnement, Sociétés et Archéologie*", Presses Universitaires Francomtoises* 3, 403–411.
1030 Edouard J-L., Thomas A., 2008. Cernes d'arbres et chronologie holocène dans les Alpes françaises.
1031 Actes de la Table ronde JurAlp "Dynamique holocène de l'environnement dans le Jura et les
1032 Alpes : du climat à l'Homme" dir. M. Desmet, M. Magny, F. Mocci, Aix en Provence, 15-16
1033 novembre 2007, Collection EDYTEM 6, Chambéry, 179–190.
1034 Ferris D.G., Cole-Dai J., Reyes A.R., Budner D.M., 2011. South Pole ice core record of explosive
1035 volcanic eruptions in the first and second millennia A.D. and evidence of a large eruption in the
1036 tropics around 535 A.D., J. Geophys. Res. 116, 1–11, doi:10.1029/2011JD015916.
1037 Finsinger W., Tinner W., 2007. Pollen and plant macrofossils at Lac de Fully (2135 m a.s.l.):
1038 Holocene forest dynamics on a highland plateau in the Valais, Switzerland. The Holocene 17, 8,
1039 1119–1127.
1040 Friedrich W.L., Kromer B., Friedrich M., Heinemeier J., Pfeiffer T., Talamo S., 2006. Santorini
1041 Eruption Radiocarbon Dated to 1627-1600 B.C. Science 312, 548.

1042 Gao C., Robock A., Ammann C., 2008. Volcanic forcing of climate over the past 1500 years: an
1043 improved ice core-based index for climate models. J. Geophys. Res. 113.
1044 doi:10.1029/2008JD010239.
1045 Gardent M., Rabatel A., Dedieu J.P., Deline P., 2014. Multitemporal glacier inventory in the French
1046 Alps from the late 1960s to the late 2000s. *Submitted Global and Planetary Change*.
1047 Gibbons A.B., Megeath J.D., Pierce K.L., 1984. Probability of moraine survival in a succession of
1048 glacial advances. Geology 12, 327–330.
1049 Giguet-Covex C., Arnaud F., Enters D., Poulenard J., Millet L., Francus P., David F., Rey P-J.,
1050 Wilhelm B., Delannoy J-J., 2012. Frequency and intensity of high altitude floods over the last 3.5
1051 ka in NW European Alps. Quaternary Research 77, 12–22.
1052 Goehring B.M., Schaefer J.M., Schlüchter C., Lifton N.A., Finkel R.C., Jull A.J.T., Akçar N., Alley
1053 R.B., 2011. The Rhone Glacier was smaller than today for most of the Holocene. Geology, 39,
1054 679–682.
1055 Goehring B.M., Vacco D.A., Alley R.B., Schaefer J.M., 2012. Holocene dynamics of the Rhone
1056 Glacier, Switzerland, deduced from ice flow models and cosmogenic nuclides. Earth and Planetary
1057 Science Letters 351-352, 27–35.
1058 Grudd H., Briffa K.R., Gunnarsson B.E., Linderholm H.W., 2000. Swedish tree rings provide new
1059 evidence in support of a major, widespread environmental disruption in 1628 BC. Geophysical
1060 Research Letters 27, 2957–2960.
1061 Guyard H., Chapron E., St-Onge G., Labrie J., 2013. Late-Holocene NAO and oceanic forcing on
1062 high-altitude alpine proglacial sedimentation (Lake Bramant, Western French Alps). The
1063 Holocene 23, 1163–1172.
1064 Haas P., 1978. Untersuchungen zur Gletschergeschichte im Val d'Anniviers. Diploma thesis,
1065 University of Zürich, 103 p.
1066 Haas J.N., Richoz I., Tinner W., Wick L., 1998. Synchronous Holocene oscillations recorded on the
1067 Swiss Plateau and at timberline in the Alps. The Holocene 8, 3, 301–309.
1068 Heiri O., Lotter A.F., Hausmann S., Kienast F., 2003. A chironomid-based Holocene summer air
1069 temperature reconstruction from the Swiss Alps. The Holocene 13, 477–484.
1070 Hoelzle M., Haeberli W., Dischl M., Peschke W., 2003. Secular glacier mass balances derived from
1071 cumulative glacier length changes. Global and Planetary Change, 36, 4, 77–89.
1072 Hoffman K.M., Smith D.J., 2013. Late Holocene glacial activity at Bromley Glacier, Cambria Icefield,
1073 northern British Columbia Coast Mountains, Canada. Canadian Journal Earth Sciences 50, 599–
1074 606.
1075 Holzhauser H., 1985. Neue Ergebnisse zur Gletscher- und Klimageschichte des Spätmittelalters und
1076 der Neuzeit. Geographica Helvetica 4, 168–185.

1077 Holzhauser H., 1997. Fluctuations of the Grosser Aletsch Glacier and the Gorner Glacier during the
1078 last 3200 years: new results. *In* Frenzel B., Boulton G.S, Gläser B., Huckriede U. (Eds) Glacier
1079 fluctuations during the Holocene. Palaoklimaforschung, 16, 35–58.
1080 Holzhauser H., 2009. Auf dem Holzweg zur Gletschergeschichte. *In* Hallers Landschaften und
1081 Gletscher. Beiträge zu den Veranstaltungen der Akademien der Wissenschaften Schweiz 2008
1082 zum Jubiläumsjahr „Haller300“. Sonderdruck aus den Mitteilungen der Naturforschenden
1083 Gesellschaft in Bern. Neue Folge 66, 173–208.
1084 Holzhauser H., 2010. Zur geschichte des Gornergletschers – Ein puzzle aus historischen dokumenten
1085 und fossilen hölzern aus dem gletschervorfeld. Geographica Bernensia, G 84. Institute of
1086 Geography, University of Bern, 253 pp.
1087 Holzhauser H., Zumbühl H.J., 1996. To the history of the Lower Grindelwald Glacier during the last
1088 2800 years - palaeosols, fossil wood and historical pictorial records - new results. Zeitschrift fur
1089 Geomorphologie Neue Folge, Suppl. Bd. 104, 95–127.
1090 Holzhauser H., Zumbühl, H.J., 2003. Jungholozäne Schwankungen des Unteren
1091 Grindelwaldgletschers. 54. Deutscher Geographentag Bern. Geographica Bernensia.
1092 Geographisches Institut der Universität Bern.
1093 Holzhauser H., Magny M., Zumbühl H.J., 2005. Glacier and lake-level variations in west-central
1094 Europe over the last 3500 years. The Holocene 15, 6, 789–801.
1095 Hormes A., Beer J., Schlüchter C., 2006. A geochronological approach to understanding the role of
1096 solar activity on Holocene glacier length variability in the Swiss Alps. Geografiska Annaler 88A,
1097 281–294.
1098 Humlum O., Solheim J., Stordahl K., 2011. Identifying natural contributions to late Holocene climate
1099 change. Global and Planetary Change 79, 145–156.
1100 Ilyashuk E.A., Koinig K.A., Heiri O., Ilyashuk B.P., Psenner R., 2011. Holocene temperature
1101 variations at a high-altitude site in the Eastern Alps: a chironomid record from Schwarzsee ob
1102 Sölden, Austria. Quaternary Science Reviews 30, 176–191.
1103 Imhof P., Nesje A., Nussbaumer S.U., 2012. Climate and glacier fluctuations at Jostedalsbreen and
1104 Folgefonna, southwestern Norway and in the western Alps from the ‘Little Ice Age’ until the
1105 present: The influence of the North Atlantic Oscillation. The Holocene 22, 2, 235–247.
1106 Ivy-Ochs S., Kerschner H., Maisch M., Christl M., Kubik P.W., Schluchter C., 2009. Latest
1107 Pleistocene and Holocene glacier variations in the European Alps. Quaternary Science Reviews
1108 28, 2137–2149.
1109 Jackson S.I., Laxton S.C., Smith D.J., 2008. Dendroglaciological evidence for Holocene glacial
1110 advances in the Todd Icefield area, northern British Columbia Coast Mountains. Canadian Journal
1111 of Earth Sciences 45, 1, 83–98.
1112 Jansen E., Overpeck J., Briffa K.R., Duplessy J.-C., Joos F., Masson-Delmotte V., Olago D., Otto-
1113 Bliesner B., Peltier W.R., Rahmstorf S., Ramesh R., Raynaud D., Rind D., Solomina O., Villalba

R., Zhang D., 2007. Palaeoclimate. In *Climate Change 2007: The Physical Science Basis. Contribution of Working Group I to the Fourth Assessment Report of the Intergovernmental Panel on Climate Change*. S. Solomon, D. Qin, M. Manning, Z. Chen, M. Marquis, K.B. Averyt, M. Tignor, and H.L. Miller, Eds. Cambridge University Press, 433–497.

Joerin U., Stocker T.F., Schlüchter C., 2006. Multicentury glacier fluctuations in the Swiss Alps. The Holocene 16, 5, 697–704.

Joerin U., Nicolussi K., Fischer A., Stocker T.F., Schlüchter C., 2008. Holocene optimum events inferred from subglacial sediments at Tschierva Glacier, Eastern Swiss Alps. Quaternary Science Reviews 27, 337–350.

Jóhannesson T., Raymond C., Waddington E., 1989. Time-scale for adjustment of glaciers to changes in mass balance. Journal of Glaciology 35, 121, 355–369.

Johnson K., Smith D.J. 2012. Dendroglaciological reconstruction of late Holocene glacier activity at White and South Flat Glaciers, Boundary Range, northern British Columbia Coast Mountains, Canada. The Holocene 22, 984–992.

Kellerer-Pirklbauer A., Drescher-Schneider R., 2009. Glacier fluctuation and vegetation history during the Holocene at the largest glacier of the Eastern Alps (Pasterze Glacier, Austria): New insight based on recent peat findings. Proceedings of the 4th Symposium of the Hohe Tauern National Park for Research in Protected Areas, Kaprun, Austria, September 2009, 151–155.

Kirkbride M.P., Brazier V., 1998. A critical evaluation of the use of glacial chronologies in climatic reconstruction, with reference to New Zealand. Quaternary Proceedings 6, 55–64.

Kirkbride M.P., Winkler S., 2012. Correlation of Late Quaternary moraines: Impact of climate variability, glacier response, and chronological resolution. Quaternary Science Reviews 46, 1–29.

Klok E.J., Oerlemans J., 2003. Deriving historical equilibrium-line altitudes from a glacier length record by linear inverse modelling. The Holocene 13, 3, 343–351.

Kobashi T., Goto-Azuma K., Box J.E., Gao C.C., Nakaegawa T., 2013. Causes of Greenland temperature variability over the past 4000 yr: implications for northern hemispheric temperature changes. Climate of the Past 9, 5, 2299–2317.

Koch, J., Clague, J.J. 2006. Are insolation and sunspot activity the primary drivers of Holocene glacier fluctuations? PAGES News 14, 20–21.

Koch J., Clague J.J., 2011. Extensive glaciers in northwest North America during Medieval time. Climatic Change 107, 593–613.

Koch J., Osborn G.D., Clague J.J., 2007. Pre-'Little Ice Age' glacier fluctuations in Garibaldi Provincial Park, Coast Mountains, British Columbia, Canada. The Holocene 17, 1069–1078.

Larsen L. B., Vinther M., Briffa K. R., Melvin T. M., Clausen H. B., Jones P. D., Siggaard-Andersen M.-L., Hammer C. U., Eronen M., Grudd H., Gunnarson B. E., Hantemirov R. M., Naurzbaev M. M., Nicolussi K. 2008. New ice core evidence for a volcanic cause of the A.D. 536 dust veil. Geophys. Res. Lett. 35, L04708, doi:10.1029/2007GL032450.

1151 Leclercq P.W., Oerlemans J., 2012. Global and hemispheric temperature reconstruction from glacier
1152 length fluctuations. Climate Dynamics 38, 1065–1079.
1153 Leemann A., Niessen F., 1994. Holocene glacial activity and climatic variations in the Swiss Alps:
1154 reconstructing a continuous record from proglacial lake sediments. The Holocene 4, 3, 259–268.
1155 Leloup P.H., Arnaud N., Sobel E.R., Lacassin, R., 2005. Alpine thermal and structural evolution of the
1156 highest external crystalline massif: the Mont Blanc. Tectonics 24, TC4002. doi:
1157 10.1029/2004TC001676
1158 Le Roy M., 2012. Reconstruction of Holocene glacier fluctuations in the Western Alps – contributions
1159 of dendrochronology and terrestrial cosmogenic nuclides dating [in French]. Unpublished PhD
1160 thesis. Université de Savoie, 360 p.
1161 Lliboutry L., Reynaud L., 1981. 'Global dynamics' of a temperate valley glacier, Mer de Glace, and
1162 past velocities deduced from Forbes' bands. Journal of Glaciology 27, 96, 207–226.
1163 Lockwood M., 2012. Solar influence on global and regional climates. Surveys in Geophysics, 33 (3-4).
1164 503-534. ISSN 1573-0956 doi: 10.1007/s10712-012-9181-3.
1165 Luckman B.H., 1995. Calendar-dated, early 'Little Ice Age' glacier advance at Robson Glacier, British
1166 Columbia, Canada. The Holocene 5, 149–159.
1167 Lukas S., Graf A., Coray S., Schlüchter C., 2012. Genesis, stability and preservation potential of large
1168 lateral moraines of Alpine valley glaciers – towards a unifying theory based on Findelengletscher,
1169 Switzerland. Quaternary Science Reviews 38, 27–48.
1170 Lüthi M.P., 2013. Little Ice Age climate reconstruction from ensemble reanalysis of Alpine glacier
1171 fluctuations, The Cryosphere Discuss. 7, 5147–5175, doi:10.5194/tcd-7-5147–2013.
1172 Magny M. 2004. Holocene climate variability as reflected by mid-European lake-level fluctuations
1173 and its probable impact on prehistoric human settlements. Quaternary International 113, 65–79.
1174 Magny M, Arnaud F, Holzhauser H., Chapron E., Debret M., Desmet M., Leroux A., Revel M.,
1175 Vannière B., Millet L., 2010. Solar and proxy-sensitivity imprints on paleohydrological records
1176 for the last millennium in westcentral Europe. Quaternary Research 73, 173–179.
1177 Martin S., 1977. Analyse et reconstitution de la série de bilans annuels du glacier de Sarennes, sa
1178 relation avec les fluctuations du niveau de trois glaciers du massif du Mont Blanc (Bossons,
1179 Argentière, Mer de Glace). Zeitschrift Fur Gletscherkunde und Glazialgeologie 13, 1-2, 127–153.
1180 Marzeion B., Nesje A., 2012. Spatial patterns of North Atlantic Oscillation influence on mass balance
1181 variability of European glaciers. The Cryosphere 6, 661–673.
1182 Marzeion B., Hofer M., Jarosch A.H., Kaser G., Mölg T., 2012. A minimal model for reconstructing
1183 interannual mass balance variability of glaciers in the European Alps. The Cryosphere 6, 71–84.
1184 Mayewski P.A., Rohling E.E., Stager J.C., Karlén W., Maasch K.A., Meeker L.D., Meyerson E.A.,
1185 Gasse F., van Kreveld S., Holmgren K., Lee-Thorp J., Rosqvist G., Rack F., Staubwasser M.,
1186 Schneider R.R., Steig E.J., 2004. Holocene climate variability. Quaternary Research 62, 243–255.

McCormick M., Büntgen U., Cane M.A., Cook E.R., Harper K., Huybers P., Litt T., Manning S.W., Mayewski P.W., More A.F.M., Nicolussi K., Tegel W., 2012. Climate Change during and after the Roman Empire: Reconstructing the Past from Scientific and Historical Evidence. Journal of Interdisciplinary History 43, 169–220.

Miller G.H., Geirsdóttir A., Zhong Y., Larsen D.J., Otto-Bliesner B.L., Holland M.M., Bailey D.A., Refsnider K.A., Lehman S.J., Southon J.R., Anderson C., Björnsson H., Thordarson T., 2012. Abrupt onset of the Little Ice Age triggered by volcanism and sustained by sea-ice/ocean feedbacks. Geophys. Res. Lett. 39, L02708. http://dx.doi.org/10.1029/2011GL050168.

Müller P., 1988. Parametrisierung der Gletscher-Klima-Beziehung für die Praxis, Grundlagen und Beispiele. Zürich, Mitteilungen der VAW/ETH-Zürich, 95.

Nicolussi K., Patzelt G., 2001. Untersuchungen zur holozänen gletscherentwicklung von Pasterze und Gepatschferner (Ostalpen). Zeitschrift für Gletscherkunde und Glazialgeologie 36, 1–87.

Nicolussi K., Schlüchter C., 2012. The 8.2 ka event – calendar dated glacier response in the Alps. Geology 40, 819–822.

Nicolussi K., Kaufmann M., Patzelt G., van der Plicht J., Thurner A., 2005. Holocene tree-line variability in the Kauner Valley, Central Eastern Alps, indicated by dendrochronological analysis of living trees and subfossil logs. Vegetation History and Archaeobotany 14, 221–234.

Nicolussi K., Jörin U., Kaiser K.F., Patzelt G., Thurner A., 2006. Precisely dated glacier fluctuations in the Alps over the last four millennia. *In* Price M.F. (Ed) Global change in mountain regions. Sapiens Publishing, 59–60.

Nicolussi K., Kauffmann M., Melvin T.M., Van Der Plicht J., Schiessling P., Thurner A., 2009. A 9111 year long conifer tree ring chronology fort he European Alps: a base for environmental and climatic investigations. The Holocene 19, 6, 909–920.

Nussbaumer S.U., Zumbühl H.J., 2012. The Little Ice Age history of the Glacier des Bossons (Mont Blanc area, France): a new high-resolution glacier length curve based on historical documents. Climatic Change 111, 2, 301–334.

Nussbaumer S.U., Zumbühl H.J., Steiner D., 2007. Fluctuations of the Mer de Glace (Mont Blanc area, France) AD 1500-2050: an interdisciplinary approach using new historical data and neural network simulations. Zeitschrift für Gletscherkunde und Glazialgeologie 40, 1–183.

Nussbaumer S.U., Steinhilber F., Trachsel M., Breitenmoser P., Beer J., Blass A., Grosjean M., Hafner A., Holzhauser H., Wanner H., Zumbühl H.J., 2011. Alpine climate during the Holocene: a comparison between records of glaciers, lake sediments and solar activity. Journal of Quaternary Science 26, 7, 703-713.

Orombelli G., Porter S., 1982. Late Holocene fluctuations of Brenva Glacier. Geografia Fisica e Dinamica del Quaternario 5, 14–37.

Osborn G., 1986. Lateral-moraine stratigraphy and Neoglacial history of Bugaboo Glacier, British Columbia. Quaternary Research 26, 171–178.

1224 Osborn G., Robinson B.J., Luckman B.H., 2001. Holocene and latest Pleistocene fluctuations of
1225 Stutfield Glacier, Canadian Rockies. Canadian Journal of Earth Sciences 38, 1141–1155.
1226 Osborn G., Menounos B., Ryane C., Riedel J., Clague J.J., Koch J., Clark D., Scott K., Davis P.T.,
1227 2012. Latest Pleistocene and Holocene glacier fluctuations on Mount Baker, Washington.
1228 Quaternary Science Reviews 49, 33–51.
1229 Osborn G., Haspel R., Spooner I., 2013. Late-Holocene fluctuations of the Bear River Glacier,
1230 northern Coast Ranges of British Columbia, Canada. The Holocene 23, 3, 330–338.
1231 Patzelt G., Bortenschlager S., 1973. Die postglazialen Gletscher- und Klimaschwankungen in der
1232 Venedigergruppe (Hohe Tauern, Ostalpen). Zeitschrift für Geomorphologie N.F. Suppl. bd. 16,
1233 25–72.
1234 Paul F., Frey H., Le Bris R., 2011. A new glacier inventory for the European Alps from Landsat TM
1235 scenes of 2003: Challenges and results. Annals of Glaciology 52, 59, 144–152.
1236 Pelfini M., Belloni S., Rossi G., Strumia G., 1997. Response time of Lys Glacier (Valle d'Aosta). An
1237 example of dendrogeomorphological and environmental study. Geografia Fisica e Dinamica
1238 Quaternaria 20, 329–338.
1239 Pichler T., Nicolussi K., Goldenberg G., Hanke K., Kovács K., Thurner A., 2013. Charcoal from a
1240 prehistoric copper mine in the Austrian Alps: Dendrochronological and dendrological data,
1241 demand for wood and forest utilisation. Journal of Archaeological Science 40, 992–1002.
1242 Rabatel A., Letréguilly A., Dedieu J.-P., Eckert N., 2013. Changes in glacier Equilibrium-Line
1243 Altitude (ELA) in the western Alps over the 1984–2010 period: evaluation by remote sensing and
1244 modeling of the morpho-topographic and climate controls. The Cryosphere.
1245 Ravanel L., Allignol F., Deline P., Gruber S., Ravello M., 2010. Rockfalls in the Mont Blanc Massif in
1246 2007 and 2008. Landslides 7, 493–501.
1247 Reichert B.K., Bengtsson L., Oerlemans J. 2001. Midlatitude forcing mechanisms for glacier mass
1248 balance investigated using general circulation models. J. Clim. 14, 3767–3784.
1249 Reimer P.J., Baillie M.G.L., Bard E., Bayliss A., Beck J.W., Blackwell P.G., Bronk Ramsey C., Buck
1250 C.E., Burr G.S., Edwards R.L., Friedrich M., Grootes P.M., Guilderson T.P., Hajdas I., Heaton
1251 T.J., Hogg A.G., Hughen K.A., Kaiser K.F., Kromer B., McCormac F.G., Manning S.W., Reimer
1252 R.W., Richards D.A., Southon J.R., Talamo S., Turney C.S.M., van der Plicht J., Weyhenmeyer
1253 C.E., 2009. INTCAL 09 and MARINE09 radiocarbon age calibration curves, 0-50,000 years Cal
1254 BP. Radiocarbon 51, 4, 1111–1150.
1255 Renner F., 1982. Beiträge zur Gletschergeschichte des Gottardgebietes und dendroklimatologische
1256 Analysen an fossilen Hölzern. Physische Geographie 8. Zürich.
1257 Reyes A.V., Clague J.J., 2004. Stratigraphic evidence for multiple Holocene advances of Lillooet
1258 Glacier, southern Coast mountains, British Columbia. Canadian Journal of Earth Sciences 41,
1259 903–918.

Reynaud L., 1993. Glaciers of Europe-glaciers of the Alps: the French Alps. *In* William Jr R.S., Ferrigno J.G. (Eds) Satellite image atlas of glaciers of the world. US Geol Surv Prof Pap 1386E, E23–E36.

Reynaud L., Vincent C., 2000. Relevés de fluctuations sur quelques glaciers français. La Houille Blanche 5, 79–86.

RinnTech, 2005. TSAP-Win. Time series analysis and presentation for dendrochronology and related application. Version 0.53. www.rinntech.com

Robock A., 2000. Volcanic eruptions and climate. Review of Geophysics 38, 2, 191–219.

Röthlisberger F., 1976. Gletscher- und Klimaschwankungen im Raum Zermatt, Ferpecle und Arolla, Die Alpen 52, 59–152.

Röthlisberger F., Schneebeli W., 1979. Genesis of lateral moraine complexes, demonstrated by fossil soils and trunks: indicators of postglacial climatic fluctuations. In Schlüchter, C. (Ed.), Moraines and Varves. Balkema, Rotterdam, 387–419.

Röthlisberger H., Haas P., Holzhauser H., Keller W., Bircher W., Renner F., 1980. Holocene climatic fluctuations - Radiocarbon dating of fossil soils (fAh) and woods from moraines and glaciers in the Alps. Geographica Helvetica 35, 5, 21–52.

Reyes A.V., Wiles G.C., Smith D.J., Barclay D.J., Allen S., Jackson S., Larocque S., Laxton S., Lewis D., Calkin P.E., Clague J.J., 2006. Expansion of alpine glaciers in Pacific North America in the first millennium A.D. Geology 34, 57–60.

Ryder J.M., Thomson B., 1986. Neoglaciation in the southern Coast Mountains, British Columbia: chronology prior to the Neoglacial maximum. Canadian Journal of Earth Sciences 24, 1294–1301.

Salzer M.W., Hughes M.K., 2007. Bristlecone Pine Tree Rings and Volcanic Eruptions over the Last 5000 Years. Quaternary Research 67, 57–68.

Schimmelpfennig I., Schaefer J.M., Akçar N., Ivy-Ochs S., Finkel R.C., Schlüchter C., 2012. Holocene glacier culminations in the Western Alps and their hemispheric relevance. Geology 40, 891–894.

Schmeits M.J., Oerlemans J., 1997. Simulation of the historical variations in length of the Unterer Grindelwaldgletscher. Journal of Glaciology 43, 152–164.

Schmidt R., Roth M., Tessadri R., Weckström K., 2008. Disentangling late-Holocene climate and land use impacts on an Austrian alpine lake using seasonal temperature anomalies, ice-cover, sedimentology, and pollen tracers. Journal of Paleolimnology 40, 453–469.

Schurer A.P., Tett S.F.B., Hegerl G.C., 2014. Small influence of solar variability on climate over the past millennium. Nature Geoscience 7, 104–108.

Schweingruber F.H., 1990. Microscopic Wood Anatomy; Structural variability of stems and twigs in recent and subfossil woods from Central Europe. 3rd edition 1990. Birmensdorf, Eidgenössische Forschungsanstalt WSL.

1296 Schweingruber F.H., 2007. Wood structure and environment, Springer Series in Wood Science.
1297 Springer, Heidelberg, 279 p.
1298 Shapiro A.I., Schmutz W., Rozanov E., Schoell M., Haberreiter M., Shapiro A.V., Nyeki S., 2011. A
1299 new approach to long-term reconstruction of the solar irradiance leads to large historical solar
1300 forcing. Astron. Astrophys. 529:A67.
1301 Six D., Reynaud L., Letréguilly A. 2001. Bilans de masse des glaciers alpins et scandinaves, leurs
1302 relations avec l'oscillation du climat de l'Atlantique nord. C. R. Acad. Sci. Paris, 333, 693–698.
1303 Steinhilber F., Beer J., Fröhlich C., 2009. Total solar irradiance during the Holocene. Geophysical
1304 Research Letters 36, L19704.
1305 Steinhilber F., Abreu J.A., Jürg Beer J., Brunner I., Christl M., Fischer H., Heikkilä U., Kubik P.W.,
1306 Mann M., McCracken K.G., Miller H., Miyahara H., Oerter H., Wilhelms F., 2012. 9,400 years of
1307 cosmic radiation and solar activity from ice cores and tree rings. PNAS 109, 16, 5967–5971.
1308 Stenchikov G., Delworth T.L., Ramaswamy V., Stouffer R.J., Wittenberg A., Zeng F., 2009. Volcanic
1309 signals in oceans. Journal of Geophysical Research 114, D16104. doi:10.1029/2008JD011673.
1310 Stuiver M., Reimer P.J., Reimer R., 2011. CALIB Radiocarbon Calibration Version 6.0.1. [WWW
1311 program and documentation]. http://radiocarbon.pa.qub.ac.uk/calib/
1312 Tegel W., Elburg R., Hakelberg D., Stäuble H., Büntgen U., 2012. Early Neolithic Water Wells
1313 Reveal the World's Oldest Wood Architecture. PLoS ONE 7 (12): e51374.
1314 Telford R.J., Heegaard E., Birks H.J.B., 2004. The intercept is a poor estimate of a calibrated
1315 radiocarbon age. The Holocene 14, 296–298.
1316 Tinner W., Theurillat J.P., 2003. Uppermost limit, extent, and fluctuations of the timberline and
1317 treeline ecocline in the Swiss Central Alps during the past 11 500 years. Arctic, Antarctic and
1318 Alpine Research 35, 2, 158–169.
1319 Thibert E., Eckert N., Vincent C., 2013. Climatic drivers of seasonal glacier mass balances: an
1320 analysis of 6 decades at Glacier de Sarennes (French Alps). The Cryosphere, 7, 47–66.
1321 Trachsel M., Kamenik C., Grosjean M., McCarroll D., Moberg A., Brázdil R., Büntgen U.,
1322 Dobrovolný P., Esper J., Frank D.C., Friedrich M., Glaser R., Larocque-Tobler I., Nicolussi K.,
1323 Riemann D., 2012. Multi-archive summer temperature reconstruction for the European Alps, AD
1324 1053–1996. Quaternary Science Reviews 46, 66–79.
1325 van Geel, B., Mauquoy, D., 2010. Peatland records of solar activity: rainwater-fed Holocene raised
1326 bog deposits in temperate climate zones are valuable archives of solar activity fluctuations and
1327 related climate changes. PAGES News 18, 11–14.
1328 Vincent C., Kappenberger G., Valla F., Bauder A., Funk M., Le Meur E., 2004. Ice ablation as
1329 evidence of climate change in the Alps over the 20th century. Journal Geophysical Research 109
1330 (D10), D10104. (10.1029/2003JD003857)
1331 Vivian R., 1975. Les glaciers des Alpes Occidentales. Allier, Grenoble, 516 p.

1332 Vollweiler N., Scholz D., Mühlinghaus C., Mangini A., Spötl C., 2006. A precisely dated climate
1333 record for the last 9 kyr from three high alpine stalagmites, Spannagel Cave, Austria. Geophysical
1334 Research Letters 33, L20703, 324 doi:10.1029/2006GL027662.
1335 Wanner H., Broennimann S., Casty C., Gyalistras D., Luterbacher J., Schmutz C., Stephenson D.B.,
1336 Xoplaki E., 2001. North Atlantic Oscillation – Concepts and studies. Surv. Geophys. 22, 321–382.
1337 Wanner H., Beer J., Bütikofer J., Crowley T.J., Cubasch U., Flückiger J., Goosse H., Grosjean M.,
1338 Joos F., Kaplan J.O., Küttel M., Müller S.A., Prentice I.C., Solomina O., Stocker T.F., Tarasov P.,
1339 Wagner M., Widmann M., 2008. Mid- to Late Holocene climate change: an overview. Quaternary
1340 Science Reviews 27, 1791–1828.
1341 Wanner H., Solomina O., Grosjean M., Ritz S.P., Jetel M., 2011. Structure and origin of Holocene
1342 cold events. Quaternary Science Reviews 30, 3109–3123.
1343 Wetter W., 1987. Spät- und Post-glaziale Gletscherschwankungen im Mont Blanc Gebiet: Untere
1344 Vallée de Chamonix-Val Montjoie. Physische Geographie 22, Zürich.
1345 Wiles G.C., D'Arrigo R.D., Villalba R., Calkin P.E., Barclay D.J., 2004. Century-scale solar
1346 variability and Alaskan temperature change over the past millennium. Geophysical Research
1347 Letters 31, L15203, doi:10.1029/200GL020050
1348 Wiles G.C., Lawson D.E., Lyon E., Wiesenberg N., D'Arrigo R.D., 2011. Tree-ring dates on two pre-
1349 Little Ice Age advances in Glacier Bay National Park and Preserve, Alaska, USA. Quaternary
1350 Research 76, 190–195.
1351 Winkler S., Hagedorn H., 1999. Lateralmoränen – Morphologie, Genese und Beziehung zu
1352 Gletscherstandsschwankungen (Beispiele aus Ostalpen und West-/Zentralnorwegen). Zeitschrift
1353 für Geomorphologie, N.F., Suppl.-Bd. 113, 69–84.
1354 Winkler S., Matthews J.A., 2010. Holocene glacier chronologies: Are 'high-resolution' global and
1355 inter-hemispheric comparisons possible? The Holocene 20, 7, 1137–1147
1356 Wipf A., 2001. Gletschergeschichtliche Untersuchungen im Spät- und Postglazialen Bereich des
1357 Hinteren Lauterbrunnentals (Berner Oberland, Schweiz). Geographica Helvetica 56, 2, 133–144.
1358 Zoller H., Schindler C., Röthlisberger H., 1966. Postglaziale Gletscherstände und
1359 Klimaschwankungen im Gotthardmassiv und Vorderrheingebiet. Verhandlungen der
1360 Naturforschenden Gesellschaft in Basel 77, 97–164.
1361 Zuo Z., Oerlemans J., 1997. Numerical modelling of the historic front variation and the future
1362 behaviour of the Pasterze glacier, Austria. Annals of Glaciology 24, 234–241.

Sample code[a]	Site[b]	Species[c]	Pith offset (n)[d]	Waney edge	Tree-ring series	MTL[e]	Dendro-date (estimated death-date)[f]	†	^{14}C labo code	^{14}C sample (tree-ring series n°)	^{14}C age BP	2σ calibration range (BC/AD)	^{14}C weighted mean[g]
MDG1-04	**7**	PICE	0	y	54	54	1926-1979 AD	****					
MDG1-02	**7**	PICE	0	y	52	52	1928-1979 AD	****	SacA 18338		-		
MDG.T25	**7**	PICE	0	y	43	43	1937-1979 AD	****	SacA 18346		-		
MDG.T22	**7**	PICE	0	y	44	44	1936-1979 AD	****					
MDG1-03	**7**	PICE	0	n	59	59+	1920-1978 AD	***					
MDG1-01	**7**	PICE	0	n	79	79+	1900-1978 AD	***	SacA 18576		-		
MDG.T21	**7**	PICE	0	n	50	50+	1929-1978 AD	***					
MDG.T24	**7**	PICE	0	n	38	38+	1940-1977 AD	***					
MDG.T26	**7**	PICE	0	n	44	44+	1933-1976 AD	***					
MDG.T23	**7**	PICE	0	n	61	61+	1915-1975 AD	***					
BAY01	**6**	PICE	0	n	292	296+	1559-1850 (1854+) AD	***					
CHAP01	**1**	PICE	0	n	215	247+	1575-1789 (1821+) AD	**	SacA 18347	96-110	310 ± 30	1487-1649 AD	1568 (1713) AD
MOTT07	**1**	PICE	0	n	141	150+	1612-1752 (1761+) AD	**					
MDG.T15	*1*	PICE	c. 100 ?	n	146	247+	(1473) 1573-1718 (1719+) AD	**					
MDG.T02	*3*	PICE	0	n	149	152+	1559-1707 (1710+) AD	**					
MDG.T94	*4*	PICE	0	n	169	172+	1523-1691 (1694+) AD	**					
MDG.T116	*1*	PICE	0	n	181	183+	1396-1576 (1578+) AD	*					
MDG1-12	**6**	PICE	c. 59	n	106	178+	(1175) 1234-1339 (1352+) AD	**					
MDG.T01	*4*	LADE	0	y	208	209	1088-1295 (1296) AD	****					
MDG1-14	**6**	PICE	c. 65	n	190	264+	(1015) 1080-1269 (1278+) AD	**	SacA 22822	137-151	800 ± 30	1184-1275 AD	1235 (1292) AD
MDG.T128	**6**	PICE	c. 25	n	145	172+	(1086) 1111-1255 (1257+) AD	***					
MDG.T130	**6**	PICE	c. 65	n	137	218+	(1035) 1100-1236 (1252+) AD	**					
MDG.T127	**6**	PICE	16	n	170	191+	(1059) 1075-1244 (1249+) AD	**					
MDG.T115	**6**	PICE	c. 200 ?	y	168	388	(861) 1061-1228 (1248) AD	****					
MDG.T09	**6**	PICE	0	n	215	217+	1025-1239 (1241+) AD	**					
MDG.T11	**6**	PICE	c. 23	n	124	148+	(1094) 1117-1240 (1241+) AD	**					
MDG1-13	**6**	PICE	0	n	280	283+	951-1230 (1233+) AD	*					
MDG.T88	**6**	PICE	2	n	97	102+	(1129) 1131-1227 (1230+) AD	*					
MDG.T14	**6**	PICE	c. 53	n	216	282+	(945) 998-1213 (1226+) AD	***					
MDG.T20	**6**	PICE	c. 100 ?	n	194	299+	(926) 1026-1219 (1224+) AD	**					
MDG.T65	*3*	PICE	0	n	83	84+	1141-1223 (1224+) AD	**					
MDG.T13	**6**	PICE	0	n	158	165+	1033-1190 (1197+) AD	**					
MDG.T12	**6**	PICE	0	n	81	82+	1110-1190 (1191+) AD	**					
MDG1-18	**6**	PICE	c. 100 ?	n	241	355+	(836) 936-1176 (1190+) AD	**	SacA 22823	104-113	925 ± 30	1026-1181 AD	1102 (1249) AD
MDG.T91	**6**	PICE	c. 25	n	286	326+	(865) 890-1175 (1190+) AD	**					
MDG.T17	**6**	PICE	0	n	64	72+	1112-1175 (1183+) AD	***					
MDG1-09	**5**	PICE	0	y	98	99	1080-1177 (1178) AD	****	SacA 22826	95-98	915 ± 30	1031-1206 AD	1108 (1111) AD
MDG.T131	**6**	PICE	c. 78	n	172	251+	(927) 1005-1176 (1177+) AD	*					
MDG.T16	**6**	PICE	c. 35	n	104	140+	(1034) 1069-1172 (1173+) AD	**					
MDG S1a	**5**	ACER				*twig*			SacA 18333		880 ± 30	1042-1221 AD	1147 AD
MDG S2a	**5**	PCAB				*twig*			SacA 18334		920 ± 35	1027-1206 AD	1107 AD
MDG S3	**5**	PICE				*twig*			SacA 18335		920 ± 30	1028-1185 AD	1105 AD
MDG S4	**5**	PICE				*twig*			SacA 18336		865 ± 30	1047-1256 AD	1169 AD
MDG1-15	**6**	PICE	c. 65	n	120	200+	(948) 1013-1132 (1147+) AD	**					
MDG1-06	**5**	PICE	0	y	252	255	866-1117 (1120) AD	****	SacA 22820	211-220	960 ± 30	1021-1155 AD	1088 (1128) AD
MDG1-11	**6**	PICE	0	n	95	101+	-	**	SacA 18341	82-91	930 ± 30	1025-1169 AD	1100 (1115) AD
MDG.T89	**6**	PICE	0	n	412	418+	666-1077 (1083+) AD	*					
MDG S5	**5**	-				*twig*			SacA 18337		985 ± 30	990-1155 AD	1067 AD
MDG.T38	*3*	PICE	c. 16	n	145	191+	(889) 905-1049 (1079+) AD	***					
MDG1-10	**6**	PICE	0	n	204	225+	806-1009 (1030+) AD	**	SacA 22821	161-174	1130 ± 30	782-989 AD	919 (977) AD
MDG1-08	**5**	PICE	c. 145 ?	n	177	323+	(567) 712-888 (889+) AD	*	SacA 22825	167-175	1225 ± 30	690-885 AD	794 (802) AD
MOTT.T10	*MOTT*	PICE	c. 65	n	117	183+	(538) 603-719 (720+) AD	*					
MDG1-16	**6**	PICE	0	n	73	78	529-601 (606+) AD	**	SacA 18343	50-54	1660 ± 30	259-529 AD	384 (411) AD
MOTT06	**3**	PICE	c. 44	y	81	125	(479) 523-603 AD	****	Beta 295447	1-4	1540 ± 30	430-591 AD	509 (588) AD
MDG.T90	**6**	PICE	c. 71	n	221	295+	(231) 302-522 (525+) AD	*					
MOTT.T06	**4**	PICE	c. 145 ?	n	93	240+	(252) 397-489 (491+) AD	**					
MOTT05	**3**	PICE	c. 30	n	285	395+	(91) 121-405 (485+) AD	***					
MDG1-20_G	**6**	PICE	0	n	302	302+	169-470+ AD	*	SacA 22827	126-135	1790 ± 30	132-331 AD	232 (399) AD
MDG.T37	*2*	PICE	0	n	139	142+	303-441 (444+) AD	**					
MDG.T39_G	*2*	PICE	c. 100 ?	y	279	379	(24) 124-402 AD	****					
MDG2-01	**8**	PICE	c. 71	n	113	217+	(184) 262-374 (400+) AD	***	SacA 22828	101-110	1690 ± 30	256-420 AD	348 (382) AD
MOTT04	**3**	PICE	0	n	145	177+	202-346 (378+) AD	***					
MDG2-06	**8**	PICE	c. 10	n	252	278+	(90) 100-351 (367+) AD	*					
MDG2-08	**8**	PICE	0	n	200	299+	52-251 (350+) AD	*					
MOTT11	**3**	PICE	0	y	348	348	10 BC-337 AD	****					
MOTT13	**3**	PICE	c. 16	n	278	311+	(2) 18-295 (312+) AD	**					
MOTT01	**3**	ACER	0	y	193	193	120-312 AD	****	Beta 338488	154-158	1680 ± 30	258-425 AD	359 (391) AD
MOTT02	**3**	PICE	0	n	127	130+	158-284 (287+) AD	***	SacA 18584	94-103	1875 ± 30	70-225 AD	138 (170) AD
MDG.T41	*2*	PICE	c. 108 ?	n	224	339+	(76 BC) 32-255 (262+) AD	*					

Sample code[a]	Site[b]	Species[c]	Pith offset (n)[d]	Waney edge	Tree-ring series	MTL[e]	Dendro-date (estimated death-date)[f]	†	^{14}C labo code	^{14}C sample (tree-ring series n°)	^{14}C age BP	2σ calibration range (BC/AD)	^{14}C weighted mean[g]
MOTT10	**3**	PICE	0	n	152	221+	12 BC-139 (208+) AD	*					
MOTT12	**3**	PICE	0	n	177	179+	23 BC-153 (155+) AD	*					
MOTT.T04	*MOTT*	PICE	0	n	105	119+	17-121 (135+) AD	**					
MDG.T93	*2*	PICE	0	n	341	368+	538-198 (171+) BC	***					
MDG5-03	**10**	PICE	0	n	353	353+	960-608+ BC	***					
MDG.T35	**10**	PICE	0	n	185	230+	838-654 (609+) BC	*					
MOTT09_G	**2**	ACER	c. 100 ?	n	277	386+	(1005) 905-629 (620+) BC	**					
MOTT08	**2**	ACER	c. 15	n	171	217+	(845) 830-660 (629+) BC	**	Beta 295448	153-157	2440 ± 30	752-407 BC	561 (513) BC
MOTT.T16	*MOTT*	PCAB	c. 5	n	148	178+	(810) 805-658 (633+) BC	*					
MDG.T108	**10**	PICE	c. 100 ?	n	153	274+	(909) 809-657 (636+) BC	**					
MDG.T03	*4*	PICE	0	n	381	393+	1035-655 (643+) BC	*					
MOTT.T15	*MOTT*	PICE	0	n	152	153+	809-658 (657+) BC	*					
MDG.T106	**10**	PICE	c. 145 ?	n	92	254+	(916) 771-680 (663+) BC	*					
MDG.T138	**10**	PICE	0	n	154	159+	822-669 (664+) BC	**					
MDG5-02	**10**	PICE	0	n	124	124+	-	**	Beta 295444	70-79	2580 ± 30	814-592 BC	758 (708) BC
MDG.T43_G	**10**	PICE	c. 71	n	225	298+	(1009) 938-714 (712+) BC	*					
MDG3-05_G	**9**	PICE	0	y	341	341	1117-777 BC	****					
MDG.T123_G	**9**	PICE	0	y	296	430+	1209-914 (780+) BC	***					
MDG.T78	**9**	PICE	0	n	208	220+	1019-812 (800+) BC	**					
MDG.T04_G	**9**	PICE	0	y	428	477	1278-851 (802) BC	****					
MDG.T05	**9**	PICE	0	n	237	242+	1046-810 (805+) BC	**					
MDG.T64	**9**	PICE	c. 10	n	91	116+	(927) 917-827 (812+) BC	**					
MDG.T83	**9**	PICE	c. 100 ?	n	229	357+	(1178) 1078-850 (822+) BC	*					
MDG.T70_G	**9**	PICE	0	n	166	174	999-834 (826+) BC	***					
MDG3-07	**9**	PICE	0	n	73	83+	-	**	Beta 295443	81-85	2660 ± 30	890-798 BC ‡	824 (813) BC
MDG3-06	**9**	PICE	0	n	92	94+	-	**	Beta 295442	88-92	2690 ± 30		
MDG.T124	**9**	PICE	c. 53	n	210	301+	(1173) 1120-911 (873+) BC	*					
MOTT.T11	*MOTT*	PICE	0	n	163	167+	1053-891 (887+) BC	*					
MDG.T82	**9**	PICE	0	n	360	391+	1280-921 (890+) BC	*					
MDG.T109	*4*	PICE	c. 145 ?	n	292	298+	(1379) 1234-943 (937+) BC	**					
MDG3-02	**9**	PICE	0	n	206	246+	1207-1002 (962+) BC	**	SacA 22824	150-159	2925 ± 30	1257-1019 BC	1131 (1047) BC
MDG.T113	**9**	PICE	c. 40 ?	n	136	180+	(1145) 1105-970 (966+) BC	*					
MDG.T79_G	**9**	PICE	0	n	233	282+	1265-1033 (984+) BC	**					
MDG.T125	**9**	PICE	c. 35	n	139	174+	(1171) 1136-998+ BC	**					
MDG5-04	**10**	PICE	0	n	74	77+	-	**	Beta 295445 Beta 295446	A: 6-15 B: 66-75	A: 2870 ± 30 B: 2910 ± 30	1131-978 BC ‡	1044 (1037) BC
MDG3-01	**9**	PICE	0	n	249	260+	1273-1025 (1014+) BC	**	SacA 18581	158-165	3040 ± 30	1406-1213 BC	1315 (1216) BC
MDG.T56	**9**	PICE	c. 35	n	96	143+	(1167) 1132-1037 (1025+) BC	*					
MDG.T84	*4*	PICE	0	n	193	214+	1250-1058 (1037+) BC	**					
MDG3-03	**9**	PICE	c. 100 ?	n	180	320+	(1369) 1269-1090 (1050+) BC	*					
MDG.T67	**9**	PICE	c. 26	n	179	248+	(1297) 1271-1093 (1050+) BC	*					
MOTT.T14	*MOTT*	PICE	c. 65	y	171	251+	(1355) 1290-1120 (1105+) BC	***					
MOTT.T09	*MOTT*	PICE	0	n	70	72+	1231-1162 (1160+) BC	*					
MOTT.T12_G	*MOTT*	PICE	c. 40	n	250	315+	(1482) 1442-1193 (1168+) BC	**					
MDG.T102	*5*	PICE	0	n	228	231+	1458-1231 (1228+) BC	**					
MDG.T114	**9**	PICE	c. 78	n	131	231+	(1460) 1382-1252 (1230+) BC	**					
MDG.T103	*5*	PICE	c. 68	n	191	266+	(1560) 1492-1302 (1295+) BC	*					
MDG.T119	**10**	PICE	0	n	234	234+	1777-1544+ BC	***					
MDG.T117	**10**	PICE	0	n	166	194+	1763-1598 (1570+) BC	***					
MDG.T118	**10**	PICE	c. 46	n	135	210+	(1779) 1733-1599 (1570+) BC	**					
MDG5-01_G	**11**	PICE	0	n	243	243+	1823-1581+ BC	***	SacA 22829	190-197	3390 ± 30	1756-1611 BC	1687 (1637) BC
MDG.T45	**11**	PICE	0	y	226	226	1806-1581 BC	****					
MDG.T51	*5*	PICE	c. 78	n	186	318+	(1900) 1822-1637 (1583+) BC	***					
MDG.T71	*5*	PICE	0	n	126	126+	1718-1593+ BC	***					
MDG.T99_G	*5*	PICE	0	n	233	298+	1892-1660 (1595+) BC	**					
MDG.T121	**11**	PICE	0	n	156	195+	1794-1639 (1600+) BC	**					
MDG.T86_G	*5*	PICE	0	n	353	380+	1985-1633 (1606+) BC	**					
MDG.T32	**11**	PICE	0	n	203	222+	1829-1627 (1608+) BC	**					
MDG.T120	**10**	PICE	22	y	165	220	(1829) 1807-1643 (1610) BC	****					
MDG.T101_G	*5*	PICE	c. 15	n	164	208+	(1827) 1812-1649 (1620+) BC	**					
MDG.T98	*5*	PICE	c. 71	n	199	300+	(1928) 1857-1659 (1629+) BC	**					
MDG.T96	*5*	PICE	c. 35	n	121	189+	(1830) 1795-1675 (1642+) BC	**					
MDG.T95_G	*5*	PICE	0	n	226	243+	1886-1661 (1644+) BC	**					
MDG.T34	**11**	PICE	c. 46	n	102	163+	(1808) 1762-1661 (1646+) BC	**					
MDG.T53_G	*5*	PICE	0	n	298	317+	1968-1671 (1652+) BC	**					
MDG.T47_G	*5*	PICE	0	y	190	202+	1856-1667 (1655+) BC	***					
MDG.T105	*5*	PICE	0	n	148	165+	1835-1688 (1671+) BC	*					
MDG.T133	*5*	PICE	146	n	317	487+	(2173) 2027-1711 (1687+) BC	*					
MDG.T132	*5*	PICE	14	n	98	134+	(1828) 1814-1717 (1695+) BC	**					
MDG.T36	*5*	PICE	0	n	116	117+	1828-1713 (1712+) BC	**					

Tab. 1. Dendrochronological and radiocarbon results for the Mer de Glace subfossil samples. [a] Sample names including ".T" are detrital tree remains coming from the talus scree. The suffix "G" indicates a grouping of several samples within a *single tree*. [b] Site indication is given for samples embedded-in-till, and for samples for which the layer of origin is accurately known or assumed based on robust topographical evidence (bold font). Regarding detrital samples for which the layer of origin has not been sampled and could not been identified, only the sector is reported (italic font). [c] PICE: *Pinus cembra*; ACER: *Acer* sp.; PCAB: *Picea abies*; LADE: *Larix decidua*. [d] "0" means that the pith is present. [e] Estimated MTL, includes PO estimates and outermost rings counting. Please note that results for the MDG.T47_G sample are reported as a *terminus post quem* at 1655+ BC, despite the presence of the waney edge. Few outermost rings just before waney edge were not accurately countable, therefore a conservative estimate was used, close to the exact death-date. † Qualitative confidence level assigned to the dendrochronological death-date estimate: * Trunk / fragment highly eroded. Number of lacking outer ring potentially important and/or counting not accurate. ** Altered peripheral rings. Unknown number of lacking rings. Good readability of counted rings. Consistency of estimates made on different radii. *** Altered peripheral rings. Good readability of counted rings. Scattered occurence of bark/waney edge indicating a limited number of lacking rings. **** Rings measured or readable up to waney edge with good accuracy, exact death-date. ‡ 2 sigma calibration range obtained through the wiggle matching of the two radiocarbon dates indicated with the OxCal 4.1 program (Bronk Ramsey et al., 2001). [f] Please note, the timescale used for the reported dates include a "year 0". [g] Dating in brackets is the radiocarbon-derived virtual death-date used for the discussion, i.e. the central point estimate + the distance to the end of the dendro-series.

Fig. 1. (A) Location of the Mont Blanc Massif (MBM), Lake Bourget (LBo), Lake Bramant (LBr) and sites of high resolution Neoglacial glacier chronologies developed in the Alps, LG: Lower Grindelwald, GA: Great Aletsch, GO: Gorner, GP: Gepatsch, PA: Pasterze. Red star: Main EACC sampling region; white areas: 2003 glacier extent (Paul et al., 2011). **(B)** Shaded-relief map of the Mont Blanc massif with present day glacier extent in blue (France, 2009: Gardent et al. (2014); Switzerland, 2003: Paul et al. (2011); Italy, 2005: RAVA data; Projection UTM 32N). Mer de Glace present and former (late Holocene) tributaries are highlighted in red, G: Gl. du Géant, Tc: Gl. du Tacul, L: Gl. de Leschaux, Tl: Gl. de Talèfre. Locations 1 to 8 (all glaciers except 3 and 4) are mentioned in the text; approximate location of Fig. 2 is delineated.

Fig. 2. Oblique aerial view of MdG forefield (view SE; 2008 orthophoto) showing the two main studied sectors of the right lateral moraine, MOTT and MDG (the latter is divided into 5 sub-sectors). RC: Rock cliff areas with *Pinus cembra* stands overlooking the RLM. Moraine sampled exposure sites are labelled from 1 to 11 (see Supplementary Materials for a complete description of the outcrops). Single wood samples are figured with coloured dots. Little Ice Age maximum extent, as 1995 AD and 2011 AD MdG terminus position are highlighted with white and black dashed lines, respectively. Horizontal distance between 1995 AD and 2011 AD frontal positions is ca. 600 m whereas total retreat between LIA maximum and 1995 AD amounts to 1.87 km. Late-LIA frontal positions in the main valley floor are not visible (bottom left corner). Approximate position of Fig. 4 is shown with dotted line and locations cited in text are indicated.

Fig. 3. Synthesis of dendrochronological and ^{14}C dating of subfossil tree remains from the MdG forefield. **(A)** Embedded-in-till and detrital wood remains released from the RLM. Exact tree death-dates (waney edge present, exact counting of outermost rings) are in bold font, virtual death-date (no waney edge and/or conservative counting of outermost rings) are in regular font. MTL: minimum tree lifespan (includes PO estimate); MRW: mean ring width for each chronology. **(B)** Dry-dead logs fallen from the rock cliff sampled on the surface of the RLM crest at BAY site (see Fig. 2 and Fig. S5F). One sample (TRI06c) is from the Trient glacier moraine crest – same setting as BAY site (see Fig. 1 for location). Bk: bark present. Note that bark is no longer present after ca. 10 yrs of exposure and waney edge after ca. 30 yrs. **(C)** Crossdating position of modern avalanched trees from Site 7 and nearby colluvium, yielding death-date in fall/winter 1979/1980 AD; series are plotted as raw ring-width data. Note the growth pattern of juvenile trees. **(D)** Main germination and burial phases (green and blue shading, respectively). Germination phases are depicted as the mean and one standard deviation of considered dates; Intensity is higher with darker frame. Burial phases timing relies on the best preserved samples which constrained culmination of the advances (dark blue vertical bars).

Fig. 4. Spatial repartition of the dated subfossil woods at MDG sector (view ENE, 2008 orthophoto). All dated samples are figured, regardless groupings made into *single tree* nor distinction between embedded-in-till and detrital woods. Length of the exposure is 1.3 km (see Fig. 2 for location). Glacier flows from right to left.

Fig. 5. Synthesis of datings from the RLM and correlation between synchronous levels. Sample locations are given in terms of depression with respect to the moraine erosion edge (upper line). Sample sites numbering is reported (upper circled numbers). Coloured lines are isochrones representing glacier margin position at the time of burial. Time of proposed glacier advances presented here (bottom panel) take into account both the dating of wood remains embedded-in-till and of detrital remains where appropriate (datings in brackets). Site 1 (LIA reworked samples) is not shown. Flow direction of the glacier is from right to left.

Fig. 6. Altitudinal variations of MdG for the last 4 ka determined from RLM dated subfossil wood layers. Historical variations since 1500 AD are not shown (see Nusbaumer et al., 2007). To ensure consistency in the representation of the different advances throughout the record, wood layers are related to the mean glacier surface altitude right from the RLM for selected reference years (right scale) rather than to the absolute distance to the moraine crest at each sampling site (see section 5.1). For each layer altitude, the absence of the glacier is depicted by the length of the bar and ranked as: possible absence (light grey shading), probable absence (medium grey shading) and certain absence (black) – based on the interpretation of the wood remains. Number of samples on which the interpretation is based is reported on the bar. Circled numbers refer to the two possible scenarios arising from the interpretation of the Site 8 samples (see Supplementary Materials and section 6.5). Altitudinal position of the Bronze Age Warm Period samples is speculative (arrows) as only detrital wood remains were sampled from this period. The samples from L1/S9 are figured according to the results of the wiggle matching of the two radiocarbon dates. LNWP: Late Neolithic Warm Period; BWP: Bronze Age Warm Period; IRWP: Late Iron Age/Roman Age Warm Period; MWP: Medieval Warm Period.

Fig. 7. Comparison of the MdG chronology with regional and global glacier records. Vertical lines represent maximum-limiting ages for MdG advances derived from the dendrochronologically-dated subfossil woods. The dashed lines stand for the late-LIA maxima (bold lines; Nussbaumer et al., 2007) and post-LIA advances (thin lines). **(A)** MdG Neoglacial chronology (this study). Note that the MdG LIA chronology from Nussbaumer et al (2007) is depicted on the same scale (light tones) albeit it consists of length variations. **(B)** Gepatschferner dendro-based Neoglacial chronology. The "+" means that the glacier likely exceeded this position to reach an unknown maximum extent (Nicolussi and Patzelt, 2001). **(C)** Great Aletsch dendro-based Neoglacial chronology (Holzhauser et al., 2005; Holzhauser, 2009). **(D)** Sheridan glacier dendro-based Late Holocene chronology (Barclay et al., 2013). **(E)** Scandinavian glaciers Neoglacial variations. ELA reconstruction for Austre Okstindbreen (northern Norway; left axis) based on lake sediments (Bakke et al., 2010). The dashed line (right axis) figures the integrated record of glacier activity in the upstream catchment of Lake Nerfloen (440 km^2, western Norway) (Vasskog et al., 2012). **(F)** Proglacial Lake Bramant (Grandes Rousses) clastic sedimentation. Anomalies of K/Ti are depicted up to 800 AD (left axis), then anomalies of Ti from 800 AD onwards (right axis). Both are interpreted as proxies for Saint Sorlin glacier activity on the selected time periods, respectively, owing to a sedimentary source change (Guyard et al., 2013). **(G)** Detrital events recorded in the Survilly peat bog (2235 m a.s.l., Fiz massif; site 4 in Fig. 1B) (David, 2010). **(H)** Terrigenous input into Lake Le Bourget (231 m a.s.l.; LBo, Fig. 1) recorded by variations of titanium content (Jacob et al., 2008; Arnaud et al., 2012). Data are smoothed with a 3-point running average. **(I)** Replication of the MdG dated subfossil wood samples. Includes PO estimate and radiocarbon-dated samples. Light brown shading represents the addition of BAY site moraine crest samples.

Fig. 8. Comparison of the MdG glacier chronology with main climate forcings and selected alpine paleoclimate proxies. **(A)** MdG Neoglacial chronology (this study). Vertical blue shading represent the periods of tree-death (depicted in Fig. 3) interpreted as maximum ages for glacier advances. **(B)** Reconstructed total solar irradiance (TSI) from ^{10}Be measured in ice cores (Steinhilber et al., 2009). Bold line is a 31-pt running mean smoothing highlighting the multi-centennial trend (original dataset is at 5-yr resolution). **(C)** NAO reconstruction based on lake sediments from southwestern Greenland (Olsen et al., 2012). **(D)** Volcanic forcing for the northern hemisphere derived from the GISP2 sulfate record. The reconstructed volcanic signals are displayed as 51-yr running means (Kobashi et al., 2013). Please note that the y axis is broken to account for the 12th century AD low values. **(E)** COMNISPA δ^{18}O record which represents the stack of 3 speleothems from the Spannagel cave (2310 m a.s.l., Zillertal, western Austria) interpreted as an annual temperature proxy (Vollweiler et al., 2006). **(F)** Maximum latewood density record of subfossil *Larix decidua* logs from the Höhenbiel bog (1960 m a.s.l., Uri, Switzerland) interpreted as a summer (AS) temperature proxy. Series is smoothed with a 31-yr binomial low pass filter (Renner, 1982). **(G)** Reconstructed summer (JJA) temperature anomalies with respect to the 1901-2000 AD period based on EACC material from the Austrian Alps (Büntgen et al., 2011). Record is smoothed with a 31-yr running mean. **(H)** Replication of the MdG dated subfossil wood samples. Includes PO estimate and radiocarbon-dated samples.

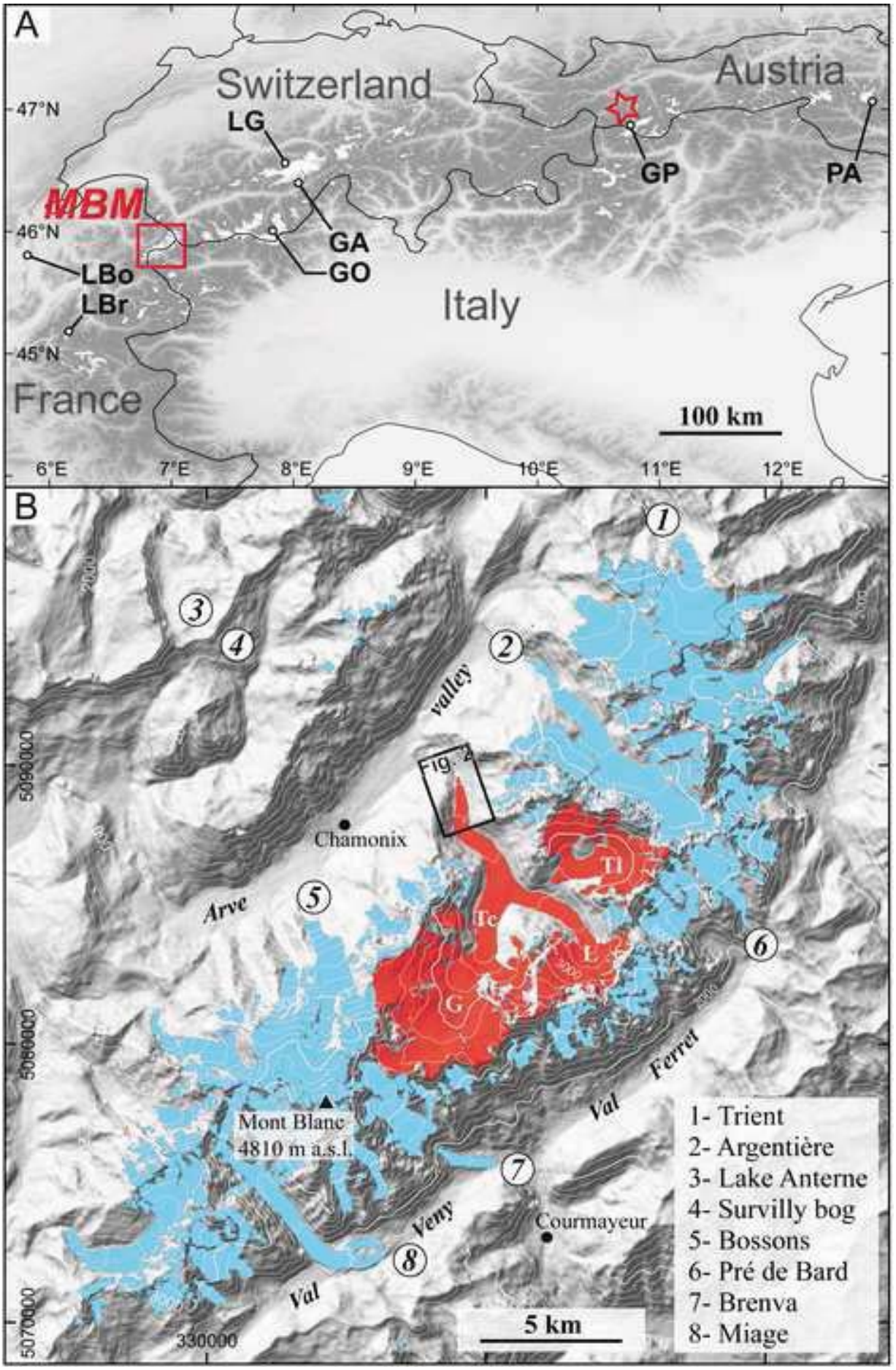
A
Switzerland
Austria
Italy
France
47°N
46°N
45°N
6°E
7°E
8°E
9°E
10°E
11°E
12°E
LG
GP
PA
MBM
GA
GO
LBo
LBr
100 km
B
1
2
3
4
5
6
7
8
valley
Fig. 2
Chamonix
Arve
Tl
Te
G
Mont Blanc
4810 m a.s.l.
Val Ferret
Veny
Val
Courmayeur
5 km
5090000
5080000
5070000
330000
1- Trient
2- Argentière
3- Lake Anterne
4- Survilly bog
5- Bossons
6- Pré de Bard
7- Brenva
8- Miage

Figure 2
Click here to download high resolution image

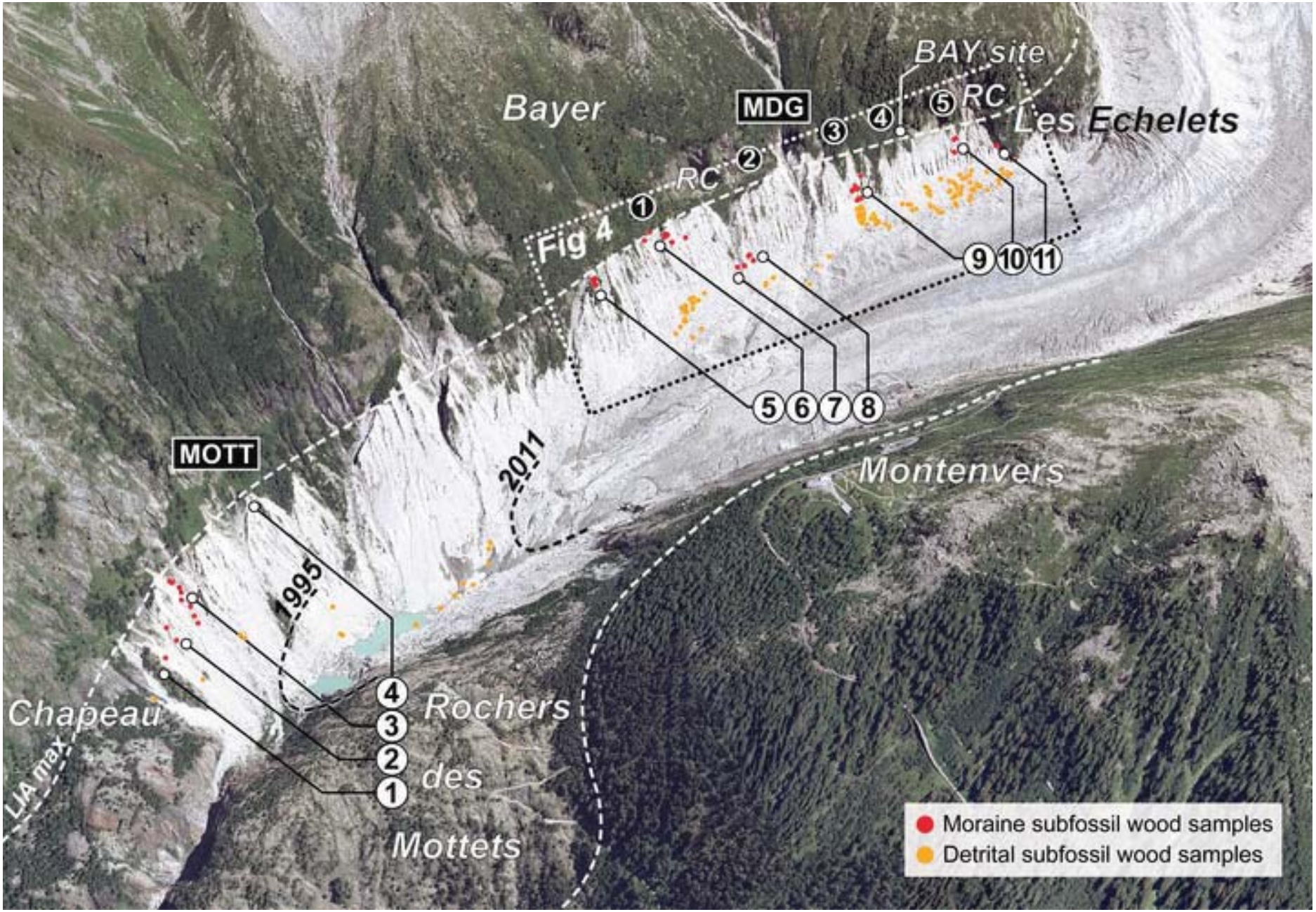

Figure 3

Click here to download high resolution image

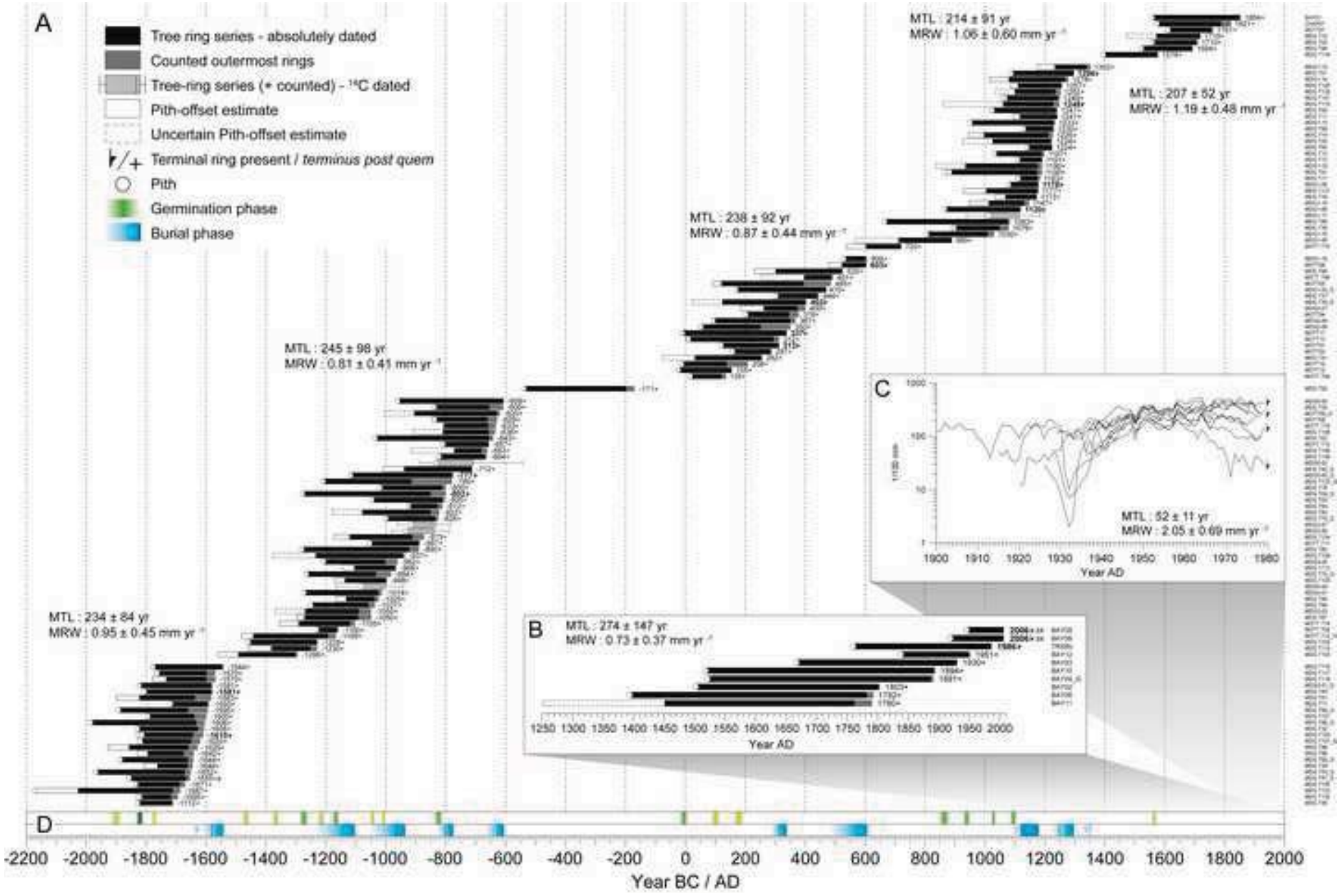

Figure 4

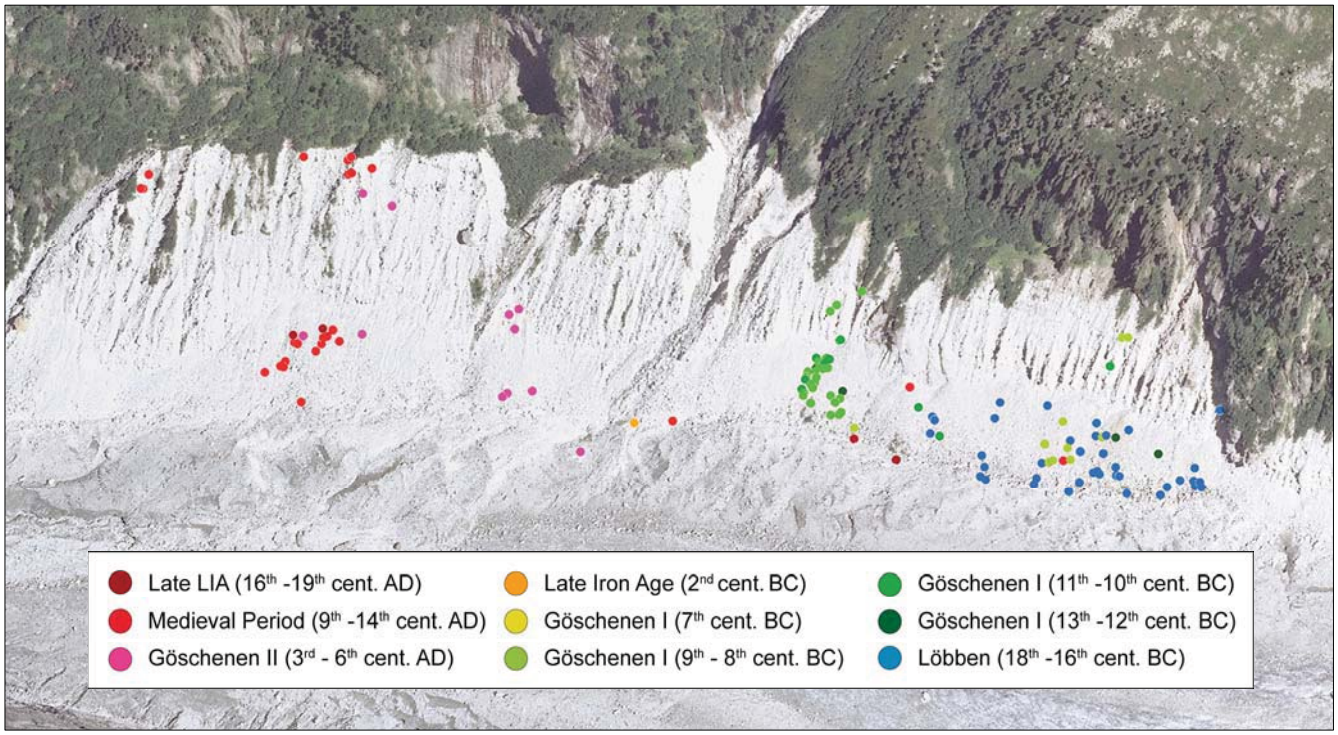
Late LIA (16th -19th cent. AD)
Medieval Period (9th -14th cent. AD)
Göschenen II (3rd - 6th cent. AD)
Late Iron Age (2nd cent. BC)
Göschenen I (7th cent. BC)
Göschenen I (9th - 8th cent. BC)
Göschenen I (11th -10th cent. BC)
Göschenen I (13th -12th cent. BC)
Löbben (18th -16th cent. BC)

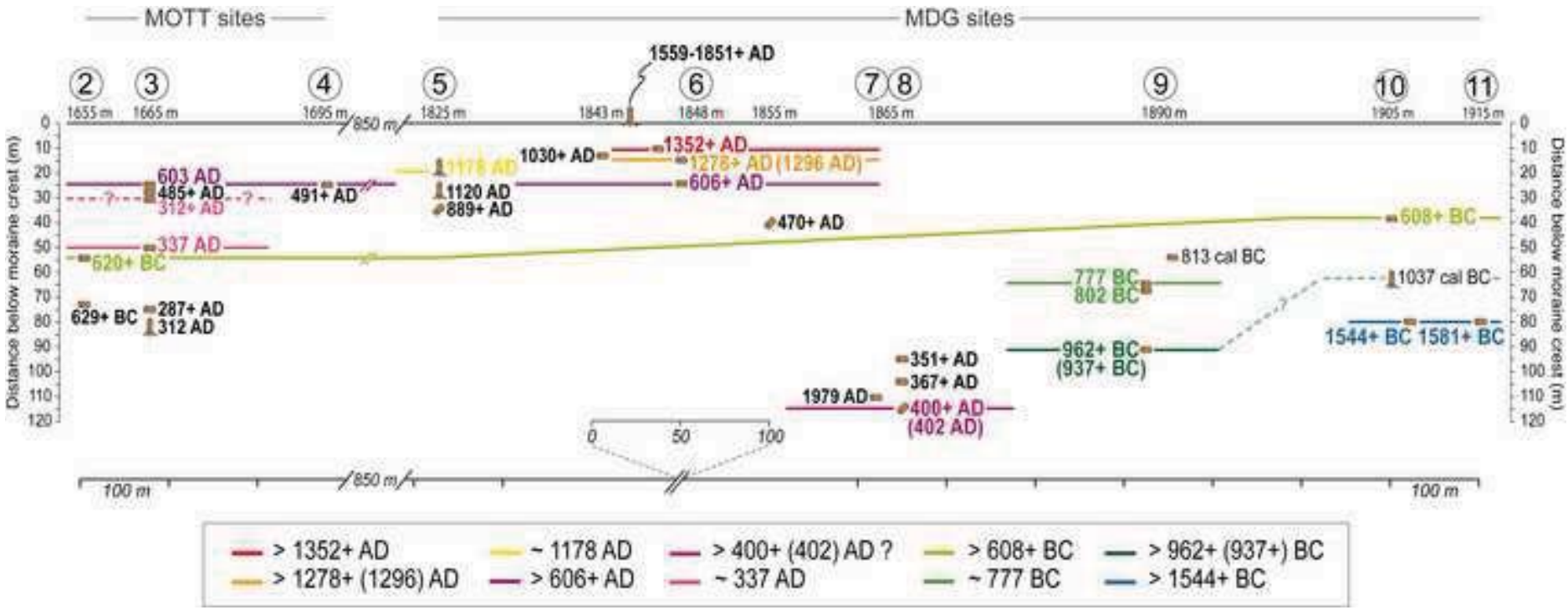
MOTT sites
MDG sites
1559-1851+ AD
2
3
4
5
6
7 8
9
10
11
1655 m
1665 m
1695 m
850 m
1825 m
1843 m
1848 m
1855 m
1865 m
1890 m
1905 m
1915 m
603 AD
485+ AD
312+ AD
491+ AD
1178 AD
1120 AD
889+ AD
1030+ AD
1352+ AD
1278+ AD (1296 AD)
606+ AD
470+ AD
608+ BC
337 AD
620+ BC
629+ BC
287+ AD
312 AD
813 cal BC
777 BC
802 BC
1037 cal BC
962+ BC
(937+ BC)
1544+ BC
1581+ BC
351+ AD
367+ AD
1979 AD
400+ AD
(402 AD)
0
50
100
100 m
850 m
100 m
Distance below moraine crest (m)
Distance below moraine crest (m)
0
10
20
30
40
50
60
70
80
90
100
110
120
> 1352+ AD
> 1278+ (1296) AD
~ 1178 AD
> 606+ AD
~ 337 AD
> 400+ (402) AD ?
> 608+ BC
~ 777 BC
> 962+ (937+) BC
> 1544+ BC

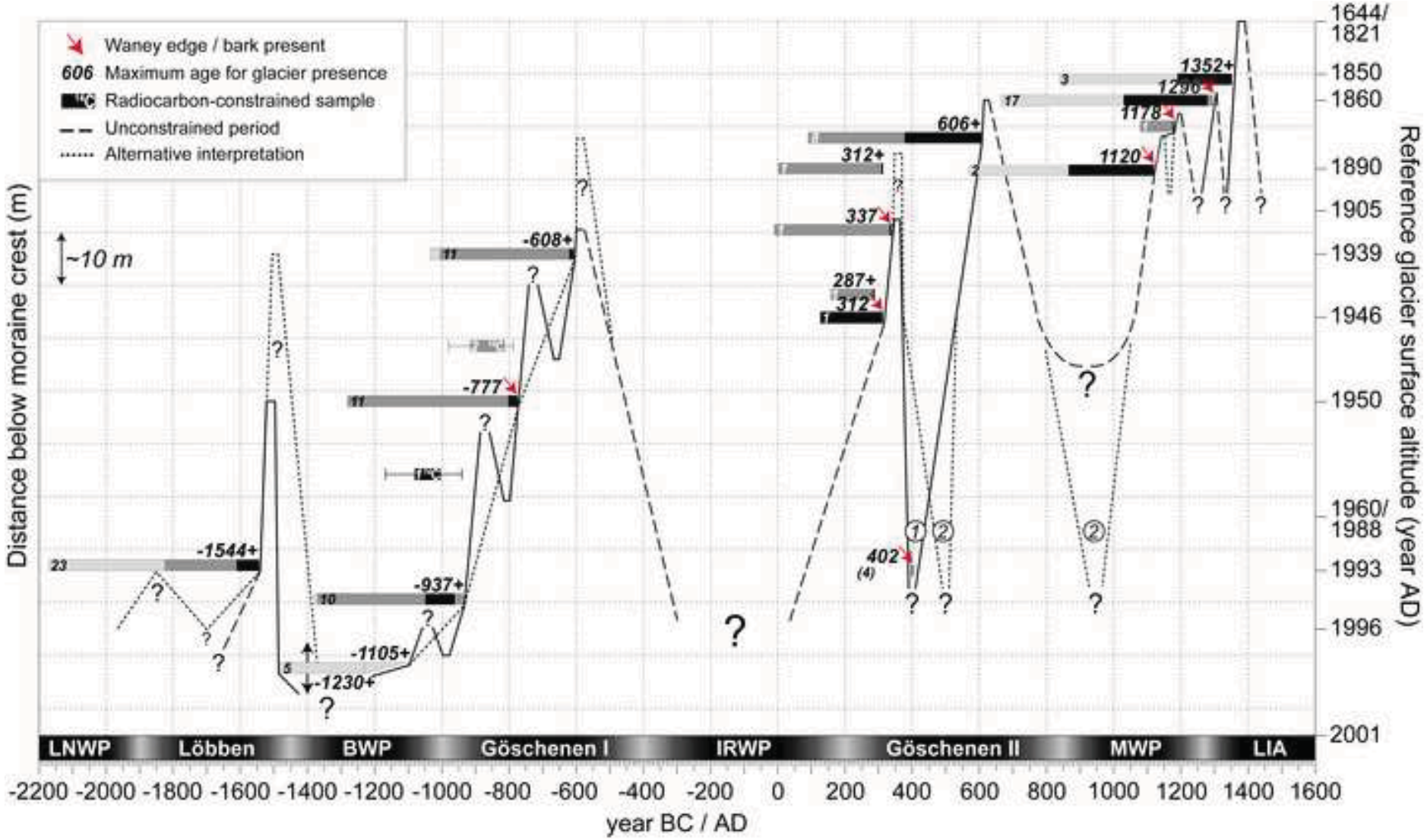
Waney edge / bark present
606 Maximum age for glacier presence
Radiocarbon-constrained sample
Unconstrained period
Alternative interpretation
~10 m
Distance below moraine crest (m)
Reference glacier surface altitude (year AD)
1644/
1821
1850
1860
1890
1905
1939
1946
1950
1960/
1988
1993
1996
2001
-1544+
-937+
-1105+
-1230+
-608+
-777
606+
312+
337
287+
312
402
(4)
1352+
1290
1178
1120
LNWP
Löbben
BWP
Göschenen I
IRWP
Göschenen II
MWP
LIA
-2200 -2000 -1800 -1600 -1400 -1200 -1000 -800 -600 -400 -200 0 200 400 600 800 1000 1200 1400 1600
year BC / AD

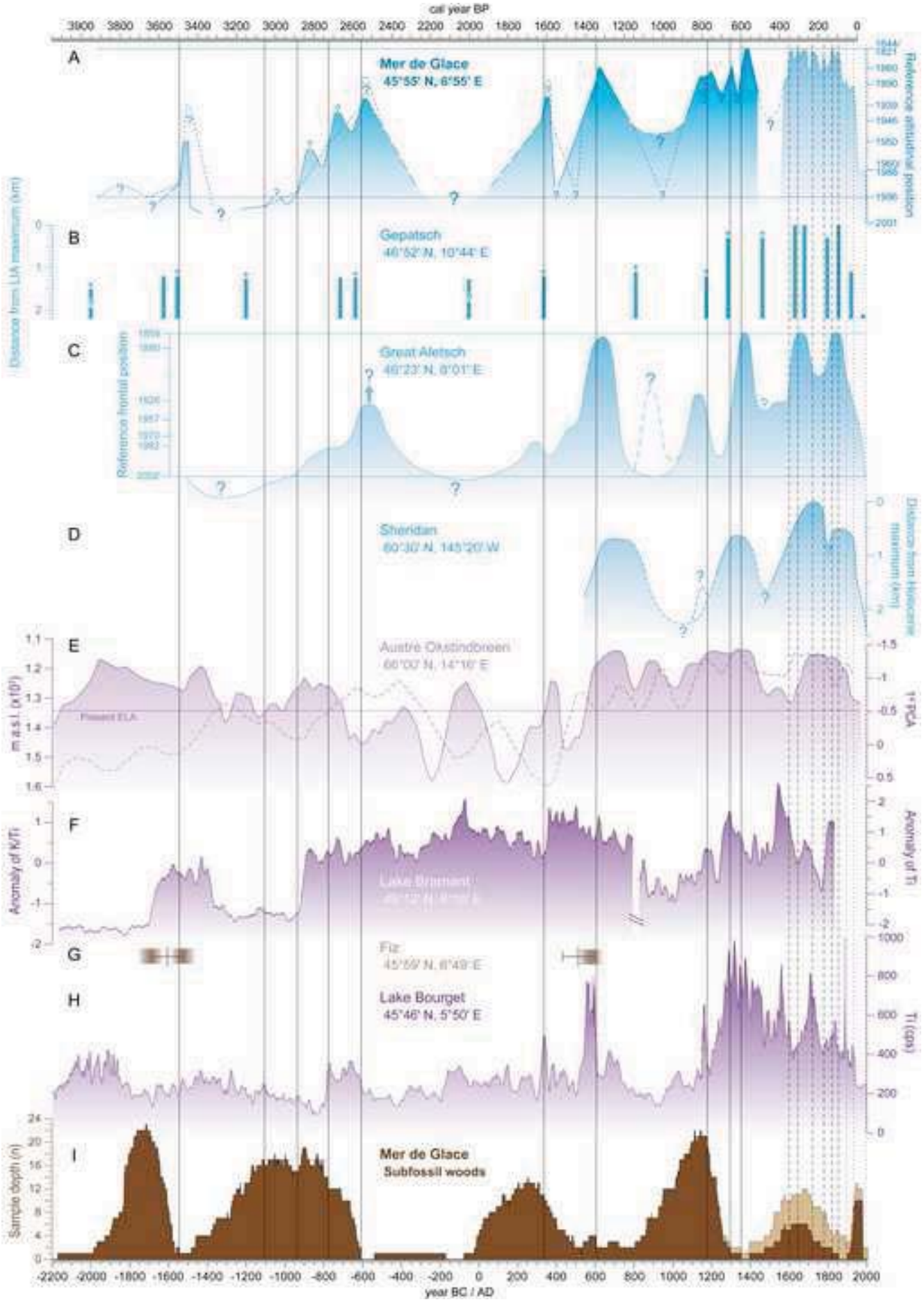
cal year BP
3900 3800 3600 3400 3200 3000 2800 2600 2400 2200 2000 1800 1600 1400 1200 1000 800 600 400 200 0
A
Mer de Glace
45°55' N, 6°55' E
Reference altitudinal position
B
Gepatsch
46°52' N, 10°44' E
Distance from LIA maximum (km)
C
Great Aletsch
46°23' N, 8°01' E
Reference frontal position
D
Sheridan
60°30' N, 145°20' W
Distance from Holocene maximum (km)
E
Austre Okstindbreen
66°00' N, 14°16' E
m a.s.l. (x10³)
Present ELA
1st PCA
F
Lake Brownell
Anomaly of K/Ti
Anomaly of Ti
G
Fiz
45°59' N, 6°49' E
H
Lake Bourget
45°46' N, 5°50' E
Ti (cps)
I
Mer de Glace
Subfossil woods
Sample depth (n)
-2200 -2000 -1800 -1600 -1400 -1200 -1000 -800 -600 -400 -200 0 200 400 600 800 1000 1200 1400 1600 1800 2000
year BC / AD

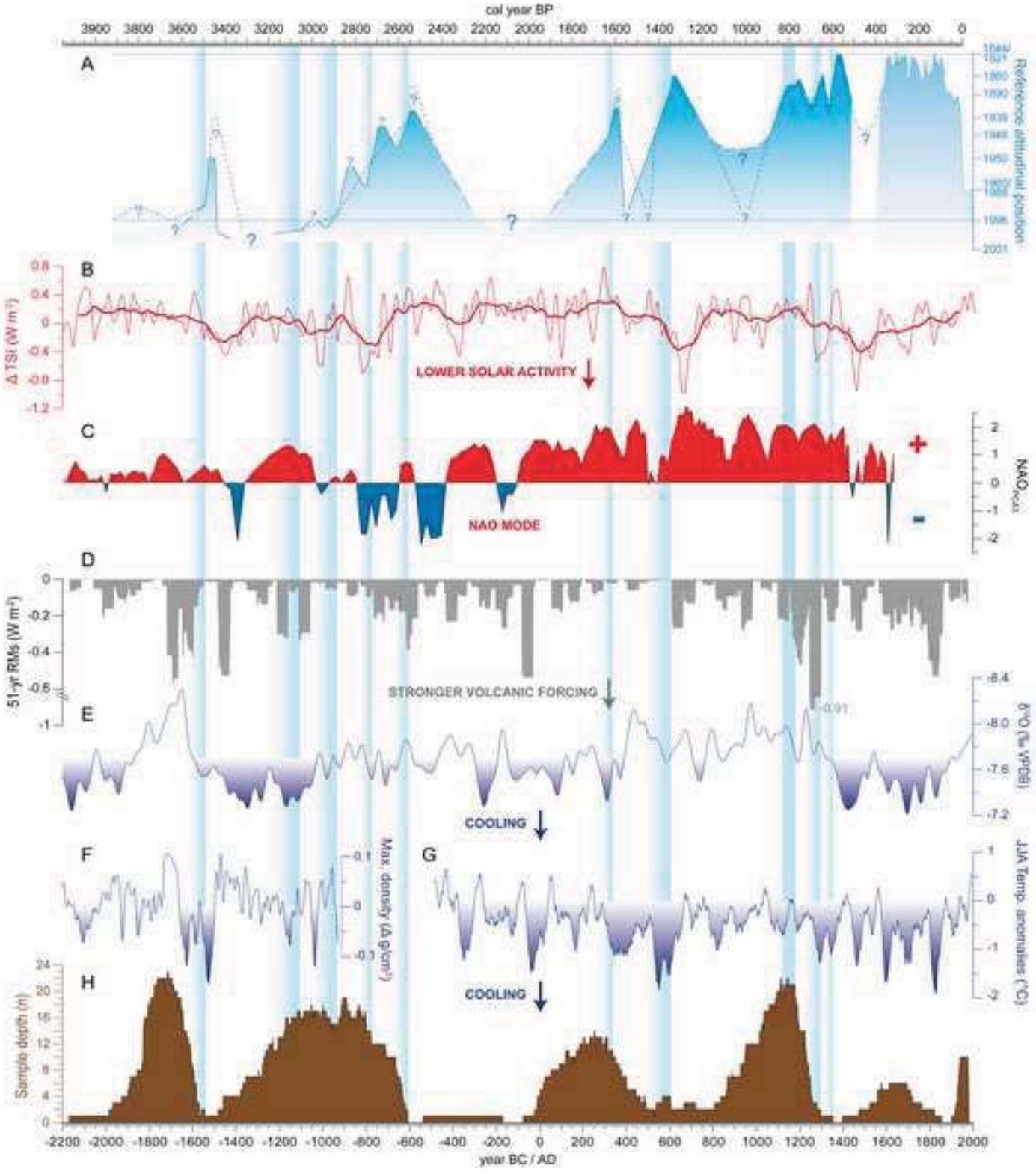
cal year BP
3900 3800 3600 3400 3200 3000 2800 2600 2400 2200 2000 1800 1600 1400 1200 1000 800 600 400 200 0
A
Reference altitudinal position
B
Δ TSI (W m⁻²)
LOWER SOLAR ACTIVITY
C
NAO MODE
+
−
NAO index
D
51-yr RMS (W m⁻²)
STRONGER VOLCANIC FORCING
E
COOLING
δ¹⁸O (‰ VPDB)
F
Max. density (Δ g/cm³)
G
COOLING
JJA Temp. anomalies (°C)
H
Sample depth (n)
-2200 -2000 -1800 -1600 -1400 -1200 -1000 -800 -600 -400 -200 0 200 400 600 800 1000 1200 1400 1600 1800 2000
year BC / AD